Received: 23 June 2022 | Revised: 29 November 2022 | Accepted: 5 December 2022

DOI: 10.1002/aoc.6983

RESEARCH ARTICLE

Applied Organometallic Chemistry WILEY

Luminescent cyclometalated platinum compounds with N, P, and O^O ligands: Density-functional theory studies and analysis of the anticancer potential

Jorge Leal[1] | **Gema Durá**[1] | **Félix A. Jalón**[1] | **Elisenda Zafon**[2] | **Anna Massaguer**[2] | **José Vicente Cuevas**[3] | **Lucia Santos**[4] | **Ana M. Rodríguez**[5] | **Blanca R. Manzano**[1]

[1]Department of Inorganic, Organic and Biochemical Chemistry—IRICA, Faculty of Chemical Sciences and Technologies, University of Castilla-La Mancha, Ciudad Real, Spain

[2]Department of Biology, Faculty of Sciences, University of Girona, Girona, Spain

[3]Department of Chemistry, Faculty of Sciences, University of Burgos, Burgos, Spain

[4]Department of Physical Chemistry, Faculty of Chemical Sciences and Technologies, University of Castilla-La Mancha, Ciudad Real, Spain

[5]Department of Inorganic, Organic and Biochemical Chemistry—IRICA, Higher Technical School of Industrial Engineering, University of Castilla-La Mancha, Ciudad Real, Spain

Correspondence
Blanca R. Manzano and Gema Durá, Department of Inorganic, Organic and Biochemical—IRICA, Faculty of Chemical Sciences and Technologies, University of Castilla-La Mancha, Avda. C. J. Cela, 10, 13071 Ciudad Real, Spain.
Email: blanca.manzano@uclm.es and gema.dura@uclm.es

Anna Massaguer, Department of Biology, Faculty of Sciences, University of Girona, Maria Aurelia Capmany 40, 17003 Girona, Spain.
Email: anna.massaguer@udg.edu

Funding information
Spanish Ministerio de Ciencia, Innovación y Universidades (MCIU), Agencia Estatal de Investigación (AEI), and Fondo Europeo de Desarrollo Regional (FEDER), Grant/Award Numbers: RTI2018-100709-B-C21, RTI2018-100709-B-C22; Junta de Comunidades de Castilla-La Mancha-FEDER (JCCM), Grant/Award Number: SBPLY/19/180501/000260; UCLM-

Luminescent platinum cyclometalated complexes are species of interest mainly due to their applications in the optoelectronic and biological fields, especially with regard to their anticancer activity. Given this level of interest, a series of cyclometalated (2-[2′-thienyl]pyridinate, thpy and 2-[2,4-difluorophenyl]pyridinate, dfppy) platinum complexes with N-donor, PTA (1,3,5-triaza-7-phosphaadamantane) or chrysin-derived ligands (incorporating piperidine, **HL1**, or morpholine, **HL2**, fragments) were synthesized. The complexes are luminescent with tunable emission wavelengths. Aggregation in solution was observed for [Pt(dfppy)L1], **5**. Density-functional theory (DFT) studies provided descriptions of the highest occupied molecular orbital (HOMO) and least unoccupied molecular orbital (LUMO) characteristics and their influence on the photophysical properties. The orbitals of **5**–**6** were different in nature to those of **1**–**4**. Time-dependent DFT (TD-DFT) calculations showed that for **1**–**4** the excited states S_1 and T_1 reflect metal-to-ligand charge transfer (MLCT) and ligand-centered (LC) (C^N) contributions while for **5**–**6** these states are an LC transition centered on **L1** or **L2**. The speciation in DMSO and DMSO/H_2O was evaluated. Biological studies showed that [Pt(thpy)Cl(Hthpy)], **1**, [Pt(dfppy)Cl(Hdfppy)], **2**, and **5** exert significant cytotoxic activity against human cervical (HeLa) and lung (A549) carcinoma cells. The cytotoxicity of **1** increased

Jorge Leal and Gema Durá have contributed in a similar way to the experimental part of the study.

FEDER, Grant/Award Numbers: 2020-GRIN-29093, 2021-GRIN-30981; European Regional Development Fund, Grant/Award Number: SBPLY/19/180501/000191; Generalitat de Catalunya, Grant/Award Number: 2021 FI_B 01036

2.84-fold upon irradiation (blue). Microscopy assays on **5** showed that this compound accumulates in cytoplasmic organelles, preferentially in mitochondria. Mitochondrial metabolism was disrupted by the activity of the complexes, leading to a decline in the adenosine triphosphate (ATP) cellular content. Overall, the results show an alternative anticancer activity for complexes **1**, **2**, and **5**, which could be of great interest for the treatment of tumors with acquired resistance to conventional DNA-targeted anticancer drugs.

KEYWORDS

anticancer, chrysin, cyclometalated, platinum, TD-DFT

1 | INTRODUCTION

Interest in luminescent platinum cyclometalated complexes has been aroused due to their applications in the optoelectronic[1–4] and biological fields,[5] amongst others. The strong ligand field produced by the σ-donating carbon atom of the metalated ring ensures a large gap between the filled d_{xy} and vacant d_{x2-y2} metal orbitals, thus ensuring that the d–d states are not energetically accessible at room temperature and minimizing the nonradiative decay. In this way, the emission from ligand centered (LC) or charge transfer states (usually MLCT, metal-to-ligand charge transfer) is more favorable. Furthermore, the cyclometalated ligands are quite kinetically inert and this imparts stability to the complexes. These properties can be fine-tuned by modifying either the cyclometalated or ancillary ligands.[6–10]

As far as biological applications are concerned, it has been reported that the complex [Pt(ppy)Cl(Hppy)] (Hppy = 2-phenylpyridine) exhibits higher cytotoxic activity than cisplatin in certain cell lines.[11] Other cyclometalated platinum derivatives have shown interesting anticancer activity,[6,12–17] including compounds with phosphane ligands.[18–22] PTA (1,3,5-triaza-7-phosphaadamantane) is a ligand that is frequently employed in anticancer complexes, including cyclometalated Pt compounds.[23–25] Although nuclear DNA is a common target in platinum (II) chemistry, in the case of Pt(II) cyclometalated complexes,[12,14,17,21,22] other targets such as cytoplasm,[6,24] nucleolus,[26] cytoplasmic structures,[13] the endoplasmic reticulum,[25] or the tubulin cytoskeletum[14,18] have been reported. Mitochondria play numerous basic functions in cells and these include adenosine triphosphate (ATP) production, regulation of cell death, and also redox balance.[27,28] Thus, mitochondria are attracting increasing interest as target organelles for killing cancer cells, especially for PDT (photodynamic therapy) treatments.[29] In particular, mitochondria-targeted agents have emerged as potential drugs to circumvent some mechanisms of resistance to chemotherapeutic drugs currently in use.[30,31] Platinum compounds that target mitochondria are not common.[27,32,33] In some cases, mitochondria-targeting ligands are introduced into the complex.[34–37] Those complexes that contain cyclometalated ligands are very scarce, and they are usually cationic.[12,38,39] Two $[Pt(C^N^N)(PPh_3)]^+$ complexes with mitochondria-specific localization have been described, and these contain a chain with a piperidine or morpholine fragment.[38,39]

An interesting approach in the field of chemotherapeutic agents with metal centers is the use of multitargeted drugs, which may combat the emergence of resistances through a dual mechanism of action. This goal can be achieved by linking bioactive ligands to the metal fragments. In this context, flavonoids are a group of naturally occurring plant phenolic compounds that exhibit interesting biological properties, including antioxidant,[40–42] anti-inflammatory, and anticancer activity.[40,43–46] The corresponding metal derivatives with flavonoid-derived ligands have also been explored as cytotoxic agents.[47,48] Some anticancer platinum complexes that contain natural[49,50] or synthetically modified[51,52] flavonoids have been reported. The natural flavonoid chrysin (5,7-dihydroxy-2-phenyl-4H-chromen-4-one),[53] along with some derivatives with different substituents at the —OH group at position 7,[40,54,55] have demonstrated pharmacological potential as anticancer agents. Although some metal complexes with chrysin derivatives have been reported,[56,57] the synthesis and study of the biological properties of platinum complexes with chrysin or chrysin-derived ligands have not been addressed. In a recent study involving Ru, Rh, and Ir complexes with chrysin-derived ligands, we observed a marked increase in cytotoxicity when a piperidine fragment was present in the flavonoid ligand.[58]

Taking into account the information outlined above, it was decided to synthesize a series of cyclometalated, 2-(2′-thienyl)pyridinate and 2-(2,4-difluorophenyl)

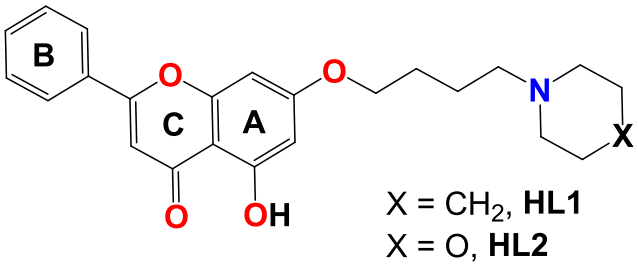

SCHEME 1 Structure of proligands **HL1** and **HL2**

pyridinate, platinum complexes with N-donor, PTA, or chrysin-derived ligands (incorporating piperidine, **HL1**, or morpholine, **HL2**, fragments, see Scheme 1). The aim was to evaluate the influence of the cyclometalated or ancillary ligands on the photophysical properties and the anticancer behavior of the complexes. Time-dependent density-functional theory (TD-DFT) studies[59] were planned as they represent a valuable tool to explain the photophysical properties and to obtain information about the orbitals involved in the absorption or emission processes. This approach makes it is easier to predict how to modulate these photophysical properties. Besides, computational studies on PTA or chrysin-derived cyclometalated Pt complexes have not previously been reported. In the case of the chrysin derivative, it was found that the ancillary ligand had an unusual effect on the orbitals involved in absorption or emission. Three of the compounds were cytotoxic against two types of cell lines and the mechanism of action involved mitochondrial dysfunction.

2 | EXPERIMENTAL

2.1 | Materials and physical methods

Unless otherwise stated, reagents and solvents were reagent quality and commercially available. Solvents and K_2CO_3 were purchased from Scharlab. Deuterated solvents were purchased from Eurisotop. $K_2[PtCl_4]$ was purchased from Johnson Matthey PLC. Hthpy and Hdfppy were purchased from Sigma-Aldrich. **HL1** and **HL2** were prepared according to the literature methods.[40,60] All synthetic manipulations were performed under an inert, oxygen-free, dry nitrogen atmosphere using standard Schlenk techniques. Solvents were distilled from the appropriate drying agents and degassed before use. Elemental analyses were performed on a Thermo Quest FlashEA 1112 microanalyzer. Analytical data for the new complexes were obtained from crystalline samples where possible. FAB^+ MS (mass spectrometry) data were recorded on a Thermo MAT95XP mass spectrometer. Multinuclear nuclear magnetic resonance (NMR) spectra were recorded at 298 K on a Varian Unity Inova 400 or on a Varian Inova 500 spectrometer. ^1H NMR chemical shifts were internally referenced to tetramethylsilane via the residual proton solvent resonances. ^{19}F and $^{31}P\{^1H\}$ NMR resonances were referenced to $CFCl_3$ and H_3PO_4 (85%), respectively. Chemical shift values are reported in parts per million and coupling constants (J) in Hertz. The splitting of proton resonances is defined as follows: s = singlet, d = doublet, t = triplet, q = quadruplet, m = multiplet, bs = broad singlet. The letters *o*, *m*, and *p* stand for *ortho*, *meta*, and *para*, respectively. COrrelation SpectroscopY (COSY) spectra were recorded using standard pulse-pulse sequences. All NMR data processing was performed using MestReNova version 6.0. Infrared (IR) spectra were registered with a Shimadzu IR-Affinity-1S spectrophotometer equipped with ATR (ZnSe prism) and the treatment of the data was performed with the software LabSolutions IR 2.11.

2.2 | Photophysical properties

Ultraviolet–visible (UV–vis) absorbance measurements were performed using a Secomam Uvikon XS spectrophotometer using the LabPower Junior program. Quartz cuvettes with 1- or 0.1-cm optical path length were used for the measurements. Fluorescence measurements were performed using PTI Quanta Mater of Photon Technology International (PTI) with a Xenon lamp (75 W) and an 814PTM detector. The samples were analyzed with the program Felix32. Products were dissolved in acetonitrile in the absence of oxygen at 10^{-5} M. The stability of the species in solution was studied at different times by monitoring the absorbance properties by UV–vis absorption. The effect of the concentration in the case of **5** was analyzed in degassed acetonitrile at concentrations in the range 10^{-4}–10^{-5} M. The quantum yield of fluorescence was calculated using the complex $[Ir(ppy)_2(bpy)]PF_6$ as reference with a quantum yield of 7.07 and applying formula 1.[61]

$$\varphi_{em,s} = \varphi_{em,ref} \frac{Area_{em,s}}{Area_{em,ref}} \cdot \frac{A_{ref}}{A_s} \quad (1)$$

where the subindexes $_s$ and $_{ref}$ correspond to the complex and the reference, respectively, $Area_{em}$ represents the area under the curve of the emission spectra, and A is the absorbance at the excitation wavelength employed in the fluorescence spectra at the same conditions: solvent, concentration, and optical length.

Photophysical properties at different solvents were performed in similar conditions as described previously. To be sure that the complexes are solved, stock solutions of 10^{-3} M in acetonitrile were prepared and then they were diluted to 10^{-5} M with dichloromethane (DCM) or

dimethylsulfoxide (DMSO), respectively, with a final ratio of solvents 1:99 (MeCN:solvent).

For the determination of the luminescence lifetime of the compounds, the fluorescence decay was measured on a PTI Time Master fluorimeter equipped with a picosecond nitrogen laser and a wavelength selector when necessary. This system was used with the dye 2-(1,1′-biphenyl)-4-yl-5-[4-(1,1′-dimethylethyl)phenyl]-1,3,4-oxadiazole (BPBD) for complex **1**. The stroboscopic detector was coupled to a Czerny–Turner monochromator on the emission port. The system was connected to a personal computer via an Ethernet interface and governed by Felix32. The instrumental parameters used were as follows: maximum λ_{exc} and λ_{em} for each compound, 300 channels, integration time = 50 μs, 10 averages per decay, 5 shots per channel, laser pulse frequency = 5 Hz, 10- or 20-nm excitation and emission slit widths, and a logarithmic collection step.

2.3 | X-ray diffraction study

Data collection for compounds **2a** and **4** was carried out on an X8 APEX II diffractometer, using Mo–Kα[62] radiation at room temperature. The data reduction was performed with the APEX31 software and corrected for absorption using SADABS.[63] Crystal structures were solved by direct methods and refined by full-matrix least-squares on F2 including all reflections using anisotropic displacement parameters by means of the WINGX crystallographic package.[64,65] All non-hydrogen atoms were refined anisotropically, and all hydrogen atoms were geometrically placed and refined using a riding model. Deposition numbers were 2181281 for compound **2a** and 2181282 for compound **4**.

2.4 | Computational studies

DFT and TD-DFT calculations were performed using Becke's three-parameter B3LYP exchange-correlation functional[66,67] implemented in Gaussian09.[68] The basis sets used to define the atoms were LANL2DZ[69] along with an f-polarization function for Pt and 6-31G(d.p)[70,71] for the other atoms. The empirical dispersion correction was taken into account using Grimme's dispersion with Becke–Johnson damping, GD3BJ.[72,73] The solvent (acetonitrile) effects were considered within the self-consistent reaction field theory using the solvation model SMD, as described by Marenich et al.[74] The geometries of the triplet states were calculated at the spin-unrestricted UB3LYP level with a spin multiplicity of 3. TD-DFT[59,75,76] calculations of the lowest-lying 10 singlets and triplets were performed in the presence of the solvent for all complexes (**1**–**6**) at the minimum-energy geometry optimized for the ground state (S_0).

2.5 | Stability experiments by NMR

Each product (1.5 mg) was dissolved in deuterated solvent (0.5 ml): DMSO-d_6 or DMSO-d_6/D_2O. For the mixtures of solvents, the ratio was 90:10 except for complex **5**, for which a ratio of 95:5 was used due to its low solubility. The evolution of ^{1}H NMR resonances was evaluated at different times to track the appearance and disappearance of different species.

2.6 | Cell lines

Human lung (A549) and cervix (HeLa) carcinoma cell lines were purchased from the American Type Culture Collection (ATCC). Cells were cultured in Dulbecco's modified Eagle's medium (DMEM) (Lonza) supplemented with 10% fetal bovine serum (FBS) (Gibco-BRL), 1 m % L-glutamine (Lonza) and 1% penicillin–streptomycin (Lonza) at 37°C in a humidified atmosphere containing 5% CO_2. Possible contamination with mycoplasma was routinely checked using the VenorH GeM Mycoplasma Detection Kit (Minerva Biolabs).

2.7 | Cytotoxicity experiments

The cytotoxic activities of the complexes were determined by the 3-(4,5-dimethylthiazol-2-yl)-2,5-diphenyltetrazolium bromide (MTT) assay. A549 or HeLa cells were seeded onto flat-bottomed 96-well plates at a density of 4000 cells per well and allowed to attach for 24 h. Complexes were first diluted in DMSO and sterile milli-Q water to prepare 1 mM stock solutions, which were then diluted in culture medium to obtain solutions ranging from 0 to 50 μM. The final concentration of DMSO in these solutions did not exceed 1%. Cells were treated for 48 h, and the cell viability was determined by the MTT assay as previously described.[77] Each treatment was tested in quadruplicate in three independent experiments. The concentration that reduced the cell viability by 50% (IC_{50}) was established for each compound using the Gen5 software (BioTek).

For photodynamic studies, cells were pre-incubated with the compounds for 4 h to enable their cellular internalization. Cells were then irradiated with a blue LED system (LuxLight) at a wavelength of 460 nm for 1 h, giving a total dose of 24.1 J cm^{-2}. The phototoxic index (PI = $IC_{50,\ dark}/IC_{50,\ light}$) of each compound was determined.

2.8 | Hemolysis assay

The hemolytic activities of the complexes were determined by measuring hemoglobin release from red blood cell (RBC) suspensions. RBCs were collected from fresh swine blood diluted to 5% v/v in phosphate-buffered saline (PBS) solution by centrifugation at 1000 rcf for 10 min and washed three times with PBS. Subsequently, RBC suspension (150 µl) was mixed with 150 µl of each complex at different concentrations (10, 25, and 50 µM). A solution of 2% Triton X-1000 in PBS was used as positive control to induce complete hemolysis. PBS alone was used as negative control. Samples were incubated for 1 h at 37°C under continuous shaking (50 rpm) and then centrifuged at 3500 rcf for 10 min. 80-µl aliquots of the supernatant were transferred to a 96-well plate and diluted with 80 µl of Milli-Q water. Hemolysis was evaluated by measuring the absorbance of the samples at 540 nm with a plate reader (BioTek, Winooski, VT, USA). The percentage of hemolysis (H) was calculated using the equation: $H = 100\ [(As - An) / (Ap - An)]$, where As is the absorbance for a given sample, An is the absorbance for the negative control, and Ap is the absorbance for the positive control. Each sample was tested in triplicate.

2.9 | Confocal microscopy

Subcellular localization of the complexes was assessed by confocal fluorescence microscopy; 100,000 HeLa or A549 cells were seeded on coverslips and allowed to attach overnight. Cells were then treated with **1**, **2**, or **5** diluted to 25 µM in DMEM without FBS. Colocalization with mitochondria was analyzed with the mitochondria-specific dye MitoTracker™ Red CMXRos (molecular probes) at 100 nM. Cells were incubated for 1 h at 37°C. The medium was removed, and cells were washed with cold PBS and fixed with 4% paraformaldehyde in PBS for 15 min at 4°C. After washing twice with PBS, the coverslips were mounted using ProLong™ Antifade Mountant (Invitrogen). Images were taken on a Nikon A1R confocal microscope and analyzed using the NIS-Elements AR (Nikon, Japan) and Fiji/ImageJ software.

2.10 | Effect on cell cycle

The effect of the complexes on cell cycle progression was studied by propidium iodide (PI) staining and flow cytometry analyses. A total of 1,000,000 HeLa cells were seeded in six-well plates and allowed to attach for 24 h. Cells were then treated with 5-µM cisplatin, 0.5-µM doxorubicin, or with complexes **1**, **2**, and **5** at the corresponding IC_{50}. After 24 h, cells were collected by trypsinization, washed with PBS, and fixed in ice-cold 70% ethanol for 24 h at 4°C. Ethanol was removed by centrifugation, and the cell pellets were washed twice with cold PBS. DNA was stained with 50 µg/ml PI (Sigma) in the presence of 50 µg/ml RNase A (Sigma). Of each sample, 20,000 cells were analyzed with a NovoCyte flow cytometer and divided into the different phases of the cell cycle (G1, S, and G2/M) according to their phase-specific DNA-content.

2.11 | ATP content measurement

The effect of the complexes on the mitochondrial function was assessed by evaluating their ability to inhibit ATP synthesis. 4000 A549 cells were seeded into opaque-walled multiwell plates and allowed to attach for 24 h. Cells were then exposed to complexes **1**, **2**, and **5** at the corresponding IC_{50} or medium alone as a control for 4 h at 36°C. ATP levels were measured with the CellTiter-Glo® luminescent assay (Promega) according to the manufacturer's instructions. Each compound was assayed in quadruplicate, and the luminescence of each well, corresponding to the ATP content, was quantified with a plate reader (BioTek, Winooski, VT, USA) and expressed as percentage relative to untreated control cells.

2.12 | Statistics

Statistical analyses were performed with the GraphPad Prism software. Quantitative variables are expressed as mean or median and standard deviation (*SD*). Statistical differences were analyzed by the Mann–Whitney non-parametric test. A value of $p < 0.05$ was considered significant.

3 | RESULTS AND DISCUSSION

3.1 | Synthesis and characterization

Complexes **1**–**6** were synthesized according to the reactions outlined in Scheme 2. Complexes **1**[12,78] and **2**[79,80] had been obtained previously, but their biological properties had not been studied, and DFT studies had not been carried out to explain their photophysical behavior. In the chrysin ligands, the —OH group at position 7 of chrysin was functionalized with alkyl chains with two different terminal groups: piperidine for **HL1** or morpholine for **HL2**. The ligands were synthesized according to

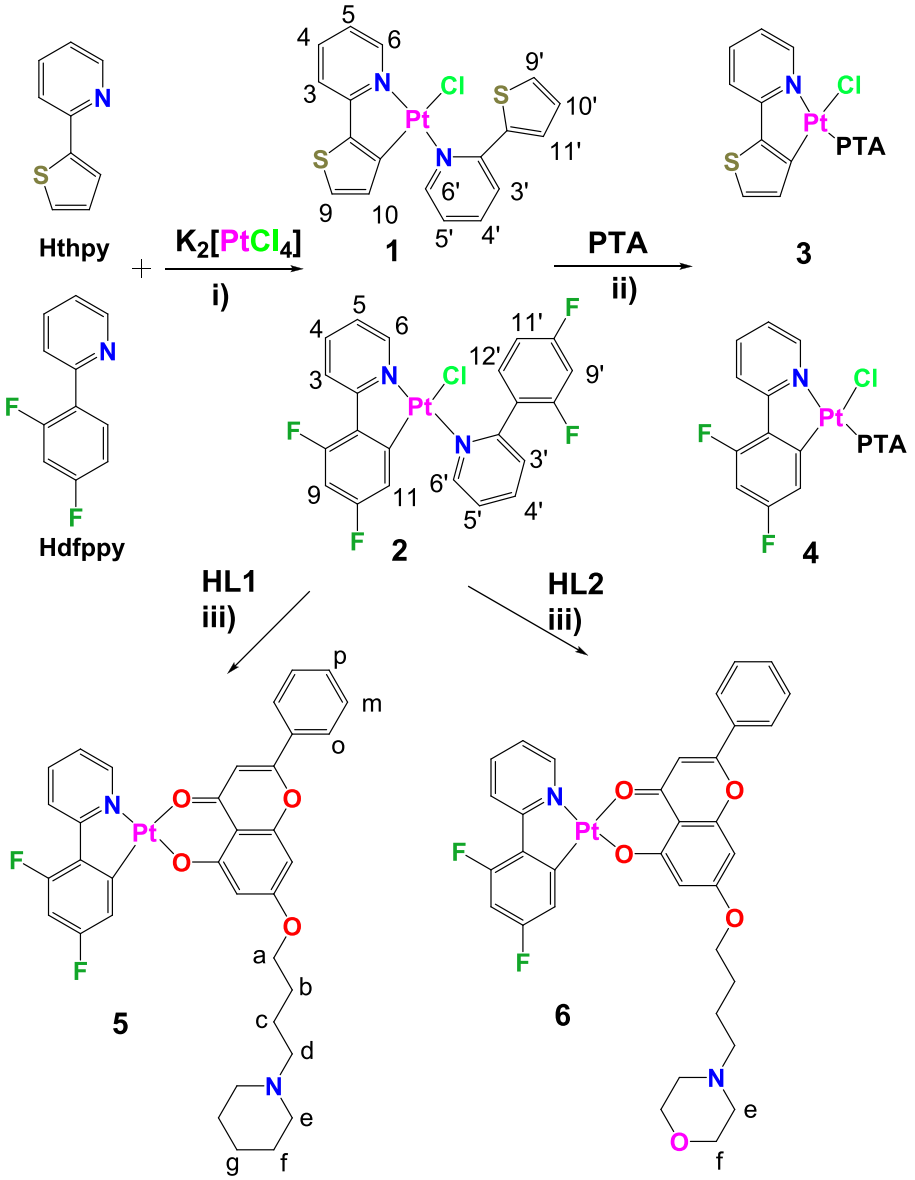

SCHEME 2 Scheme for the synthesis of complexes **1**–**6** and atom numbering scheme. (i) ethoxyethanol: water (3:1) 80°C, (ii) $CHCl_3$, and (iii) KOH, CH_2Cl_2.

literature procedures.[40,60] Complexes **1** and **2** were prepared from $K_2[PtCl_4]$ and 2-(2′-thienyl)pyridine (Hthpy) or 2-(2,4-difluorophenyl)pyridine (Hdfppy), respectively. The reactions of these compounds with PTA led to the displacement of the monodentate N-donor ligands by the phosphine and compounds **3** and **4** were obtained. The deprotonation of **HL1** or **HL2** with KOH and reaction with **2** yielded derivatives **5** and **6**, respectively. The isomers proposed for complexes **1**–**4** are consistent with the higher *trans* influence of the cyclometalated rings and the lower *trans* influence of the chloride ligand. The *trans* disposition of the C and N atoms was confirmed in the structure determined by X-ray diffraction for **1**,[78] for the similar complex with phenylpyridinate,[11] and for **4** and [Pt(dfppy)Cl(DMSO)], **2a**, both of which are reported here. The NMR data also support this ligand arrangement (see below).

Complexes were characterized by elemental analysis, mass spectrometry, and multinuclear NMR spectroscopy in $CDCl_3$ (see Figures S1–S35). The mass spectra contained envelope peaks with an *m/z* ratio and isotopic distribution compatible with the $[M]^+$ cations. In addition, the $[M—Cl]^+$ fragments were also detected for **1** and **2**. In the IR spectra of **5** and **6** bands, assigned to ν(C═O) and ν(C—O) vibrations, were found.

On the basis of ^{1}H-^{1}H-COSY experiments and prior knowledge, nearly all of the ^{1}H NMR resonances were assigned (see Figure 1 and Tables S1 and S2 for a comparison of the chemical shifts of the resonances of complexes and those of the Hthpy and Hdfppy ligands). Proton H^6

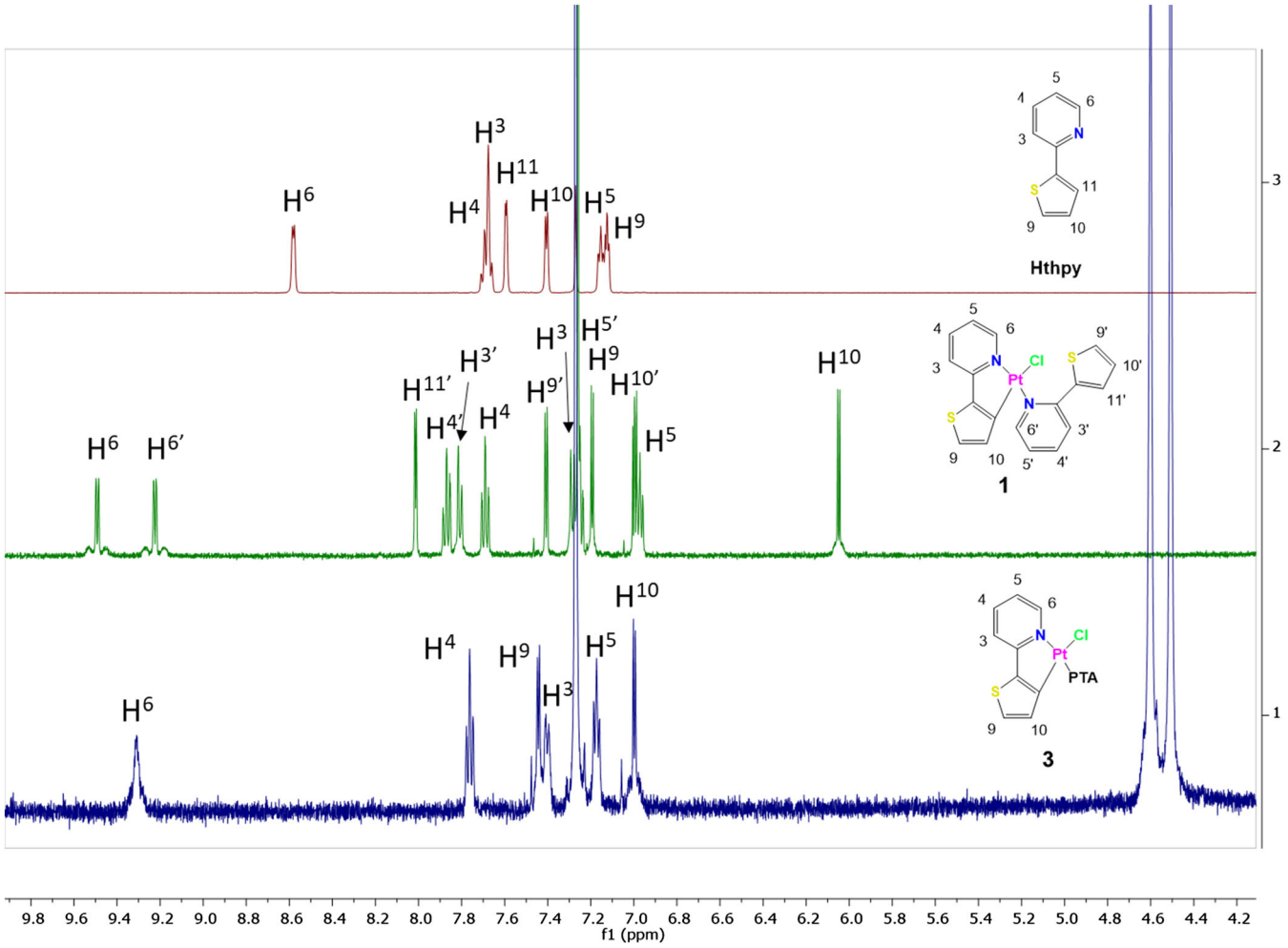

FIGURE 1 Selected region of the ^{1}H nuclear magnetic resonance (NMR) spectra ($CDCl_3$) of the proligand Hthpy and the corresponding complexes **1** and **3**.

was most strongly affected by coordination, and this was shifted to much lower field with respect the signals of the free ligands. It is worth to note the broad ^{195}Pt satellites due to $^{3}J_{195_{Pt-H}}$ coupling, with values that depend on the specific ring and are in accordance with reported values.[6] The $J_{195_{Pt-H}}$ couplings were not clearly observed for complexes **5** and **6**. Remarkably, in the cases of complexes **1** and **2**, the resonances of the proton of the CH group adjacent to the cyclometalated carbon appeared to be highly shielded (6.05 ppm for H^{10} in **1** and 5.67 ppm for H^{11} in **2**). This observation is probably due to the effect of the ring current anisotropy of the pyridine ring of the nonmetalated ligand, a fact that reflects a preferential orientation of the mono-coordinated ligand, even in solution. Coincidentally, in the structure of **1**, as determined by X-ray diffraction,[78] a weak CH–π interaction between H^{10} and the pyridine ring of the Hthpy ligand was observed. For complexes that do not contain a ligand with this pyridine ring, the signal for the corresponding proton appears at around 7 ppm.

A singlet at around −65 ppm was observed for complexes **3** and **4** in the ^{31}P{^{1}H} NMR spectrum, and this signal was shifted to lower field with respect to that of free PTA (−101.9 ppm). The value is similar to those reported for other PTA cyclometalated Pt complexes.[23,24] ^{195}Pt satellites with coupling constants $^{1}J_{Pt\text{-}P}$ of 3743 and 3769 Hz were detected in the cases of **3** and **4**, respectively. The high value for these coupling constants is consistent with the *trans* disposition of the phosphine ligands with respect to the N atom.[81]

The ^{19}F NMR spectra contained the expected resonances for complexes **3**–**6** (in general a quartet for F^{10} or $F^{10'}$ and a triplet for F^{8} or $F^{8'}$). These signals were transformed into doublets in the case of ^{19}F{^{1}H} NMR spectra (Figure S1). The coupling of $F^{10'}$ or $F^{8'}$ with $H^{12'}$ for the nonmetalated ligand (Hdfppy) was also observed in

2 (Figure S2 for $F^{10'}$). Broad ^{195}Pt satellites were detected for both types of F atoms in complexes **2** and **4** (see Figure S1).

TABLE 1 Selected bond distances (Å) and angles (°) for **4** and **2a**

Complex 4		**Complex** 2a	
Pt(1)—C(1)	2.01(1)	Pt(1)—C(1)	2.000(5)
Pt(1)—N(1)	2.091(8)	Pt(1)—N(1)	2.052(5)
Pt(1)—P(1)	2.212(3)	Pt(1)—S(1)	2.222(2)
Pt(1)—Cl(1)	2.379(3)	Pt(1)—Cl(1)	2.380(2)
N(1)—Pt(1)—Cl(1)	93.8(3)	N(1)—Pt(1)—Cl(1)	92.7(1)
P(1)—Pt(1)—Cl(1)	88.9(1)	S(1)—Pt(1)—Cl(1)	89.96(6)
C(1)—Pt(1)—N(1)	80.0(4)	C(1)—Pt(1)—N(1)	80.1(2)
C(1)—Pt(1)—P(1)	97.3(3)	C(1)—Pt(1)—S(1)	97.3(2)

3.2 | Solid-state structure of 4 and (Pt [dfppy]Cl [DMSO]), 2a

The molecular and crystal structures of complexes **4** and **2a** (formed on studying the stability of **2** in solution, see below) were determined by X-ray diffraction. The structure of **2a** confirms our proposal for the evolution of **2** in DMSO. Complex **4** crystallizes in the orthorhombic system and in the space group Pbcm and **2a** in the triclinic system and space group P-1. Selected bond distances and angles are gathered in Table 1, and the corresponding crystallographic data are compiled in Table S3. The ORTEP representation is provided in Figure 2. As one would expect, the arrangement around the platinum center is a distorted square-planar geometry formed by the cyclometalated ligand, a chloride ligand, and the phosphorus atom of the PTA ligand in the case of **4** and the S atom of DMSO for **2a**. In both complexes,

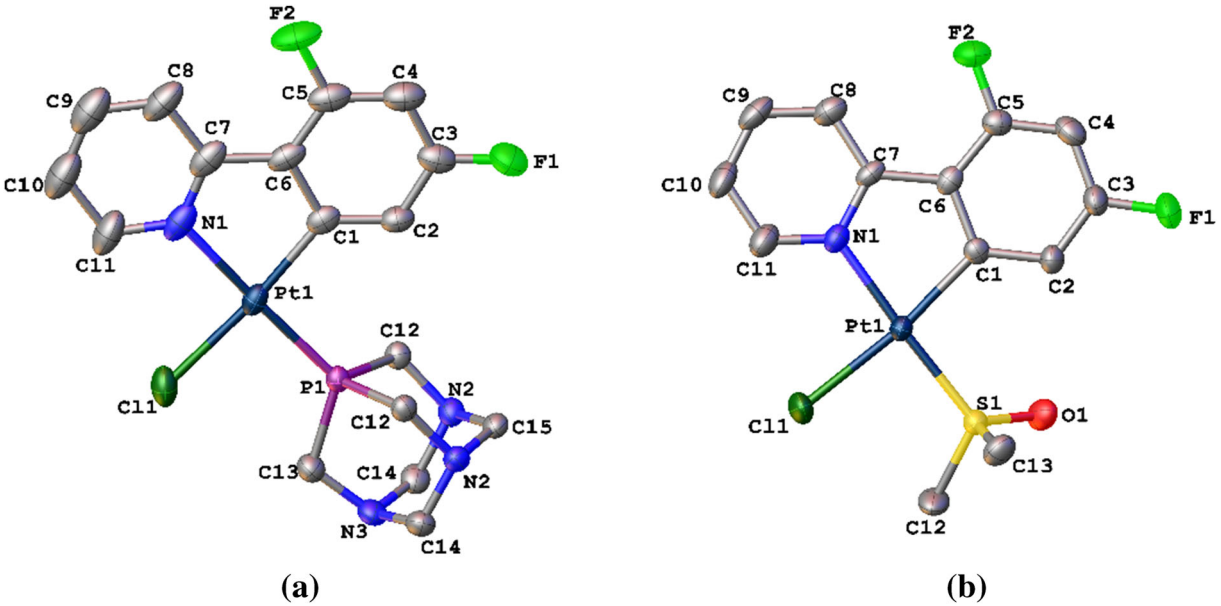

FIGURE 2 Molecular structures of complexes **4** (a) and **2a** (b). H atoms are omitted for clarity. Ellipsoids at the 30% level.

TABLE 2 Selected photophysical properties of complexes **1**–**6** in acetonitrile

Complex	**Absorbance, λ/nm (ε/10^3 M^{-1} cm^{-1})**	**ε/M^{-1} cm^{-1}/ (at 460 nm)**	**λ_{em}/nm (λ_{exc}/nm)**	**ϕ_{PL} (%)**	**τ (ns)**
1	256 (31.75), 281 (24.24), 305 (22.50), 335 (9.65), 381 (7.49), 420 (1.76)	710	567^{max}, 616 (382)	6.8	1592 ± 1.070
2	321 (11.93), 339 (6.28), 378 (2.88), 400 (3.20)	3	395, 421^{max} (337)	4.3	2.382 ± 0.03755
3	276 (11.26), 300 (12.74), 382 (2.16), 440 (0.30)	130	568^{max}, 606 (330)	0.9	1658 ± 2.013
4	270 (17.08), 322 (9.07), 338 (4.25), 350 (3.1), 374 (2.04), 400 (2.30)	1	393^{max}, 415 (336)	0.2	2.069 ± 0.02399
5	262 (45.13), 370 (8.13), 440 (2.29)	1490	557^{sh},597^{max} (262)	0.9	127.7 ± 5.897
6	260 (19.36), 302 (11.45), 366 (7.13), 450 (1.68)	1106	579 (372)	0.9	n.m.

the chloride ligand is *trans* to the difluorophenyl ring, as also found in complexes **1**[78] and **2**,[80] and, as explained above, this is consistent with the respective *trans* influence of the ligands. The bite angle of the cyclometalated ligand is 80.0(5)° in **4** and 80.1(2)° in **2a** and the torsion angle of this ligand (C[1]–C[6]–C[7]–N[1]) is 0.0° in **4** and 2.5° in **2a**, thus confirming the planarity. The Pt—C, Pt—Cl, and Pt—N distances are standard[6,18,78,82]; the Pt—P distance is similar to those found in other platinum PTA-containing complexes[23–25]; and the Pt—S distance is also similar to those in other Pt-DMSO derivatives.[83,84]

In the 3D-structure, a double π–π stacking interaction between pairs of molecules in a head-to-tail orientation is observed in both complexes, and this leads to the formation of columns with an A–B–A–B disposition that extend along the *c* axis for **4** and the *a* axis for **2a** (see Figures S36–S37 and Table S4). However, the pairs of rings involved are different: pyridine–pyridine and difluorophenyl–difluorophenyl in **4** and pyridine–difluorophenyl (×2) in **2a**. Hydrogen bonds are also formed between the chloride ligand and F, N, or O atoms as H-bond acceptors and different CH groups as H-bond donors.

3.3 | Photophysical properties

The UV–vis absorption spectra of **1**–**6** in acetonitrile were recorded (Figure S38), and the data are summarized in Table 2. The spectra contain high-energy bands ($\lambda < 330$ nm, approximately) that are dominated by spin-allowed ^{1}LC ligand-based (C^N, HC^N) $\pi \rightarrow \pi^*$ transitions.[12,18,78] Low-energy bands with moderate intensity and a λ_{max} in the range 330–390 nm were also observed, and these are typical of cycloplatinated systems.[6] According to theoretical studies (see below), these low-energy absorptions, in the cases of complexes **1**–**4**, can be classified as a combination of ^{1}MLCT (Pt to C^N), ^{1}LC (C^N), and ^{1}LLCT (Cl to C^N in **1**, **2**, and **4** or PTA to C^N in **3**) transitions. In the case of **5** and **6**, the transition is mainly ^{1}LC (**L1** for **5** and **L2** for **6**) with some contribution of ^{1}MLCT (Pt to **L1** [**5**] or **L2** [**6**]).

On comparing **1** and **2** (or **3** and **4**) a blue shift was observed for the complexes with the dfppy ligand, and this is consistent with a decreased HOMO energy level due to the presence of the electron-withdrawing fluoro-substituents. There are bands of lower energy that tail off beyond 400 nm, and these have higher intensities for complexes **1**, **5**, and **6**. (Figure S38)

Complexes **1**–**6** were emissive in degassed acetonitrile at room temperature. The excitation and emission spectra are shown in Figure 3, and the data are gathered in

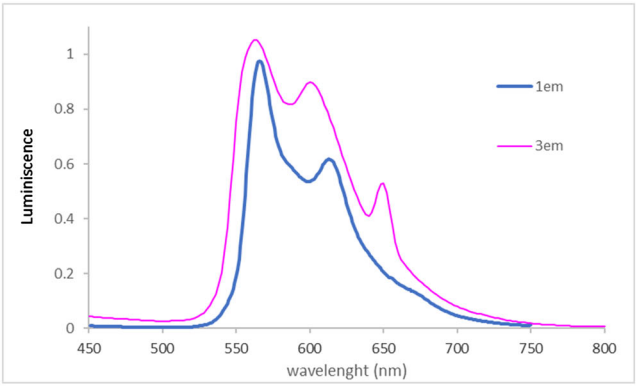

FIGURE 3 Emission spectra of complexes **1**–**6** in degassed acetonitrile (10^{-5} M) at room temperature. The bands at 372–373 nm for **2** or **4** are Raman peaks, and the peak at 652 nm for **3** is second-order artefact.

Table 2. Structured bands can be observed for **1**–**5**, and the structure is clearer for complexes **1** and **3**. As one would expect, the emission for the dfppy derivatives (**2** and **4**, 400–430 nm) was blue-shifted with respect to the corresponding thpy complexes (**1** and **3**, 560–600 nm).[78] The emissions of **5** and **6** were clearly different to that of the dfppy congeners **2** and **4**, and the maximum is observed at 597 nm (**5**) or 579 nm (**6**). The ϕ_{PL} values range from 0.2% to 6.8%.

The lifetimes of the thpy complexes (Table 2) were long, 1592 and 1658 ns for **1** and **3**, respectively, reflecting phosphorescence while for the equivalent derivatives with dfppy that exhibited emissions of higher energy, they were in the order of nanoseconds (2.382 and 2.069 ns for **2** and **4**, respectively), a fact that reveals a process of fluorescence. The distinctive feature of **5**, as compared with the other dfppy complexes, is also reflected in a value of lifetime of 127.7 ns.

The UV–vis absorption and emission spectra of **1**–**5** were also recorded in other solvents as DCM and DMSO (Figures S39–S43 and Table S5) in order to give support

to the nature of the transitions. For **1**–**4**, the charge transfer character of the low-energy bands in the UV–vis absorption (^{1}MLCT and ^{1}LLCT) and in the emission bands (^{3}MLCT and ^{3}LLCT, see below in Section 3.4) spectra fits with the dependence of the band position with the solvent. The ^{n}MLCT component was higher for **2** and **4**, and this is consistent with a more marked solvent effect than for **1** and **3**. Coincidentally, the predominantly ^{n}LC character of the transitions in the case of **5** is in accordance with the very small effect of the solvent polarity in the position of the bands.

The possible occurrence of aggregation phenomena was investigated by carrying out a concentration dependence UV–vis absorbance study in acetonitrile for one of the most planar complexes, namely, **5** (from 10^{-5} to 10^{-4}, because it was not possible to obtain more concentrated solutions, Figure 4 and S44). On increasing the concentration, similar plots for the absorbance at $\lambda = 262$, 302, or 366 nm were obtained, and it was observed that at the two highest concentrations (8×10^{-5} and 10^{-4} M) the Beer–Lambert law was not followed. This finding is due to aggregation, possibly by π–π stacking and/or Pt–Pt interactions in the ground state. New bands that could be assigned to dimer or oligomer transitions were not observed in the spectra, and the aggregates therefore could absorb at the same wavelengths but with lower molar absorptivity than the monomers or formation of microaggregates in suspension could take place (the possibility that the aggregates do not absorb cannot be conclusively ruled out, but it seems very unlikely). It is interesting to note that even for complex **4**, with a PTA ligand that disrupts the planarity, π–π stacking was found in the solid state.

The effect of the concentration on emissive behavior was examined for complex **5** in degassed acetonitrile. The emission and excitation spectra are gathered in Figure S45, and the normalized emission is provided in Figure S46. It was observed that upon increasing the concentration, the emission increased up to 8×10^{-5} M, but at 10^{-4} M, a decrease was observed. Furthermore, there was a small blue-shift of the maximum of the emission. A red-shift is usually observed in such cases due to the metal–MLCT nature of the emission.[85,86] However, the special composition of the HOMO-1 and LUMO in **5** (see below) may account for the unusual behavior observed for this complex. The same change in intensity was found in the excitation spectra. Interestingly, the pattern of the excitation spectrum changed markedly at concentrations above 6×10^{-5} (Figure S45). These findings suggest the existence of aggregates, at least in the ground state—as concluded from the absorbance studies.[24,87]

3.4 | Theoretical studies

In an effort to enhance our understanding of the photophysical properties of these compounds, DFT and TD-DFT calculations were carried out for complexes **1**–**6** (see section 2 for details). Some relevant information is provided in Table S6, and more detailed data are given in Table S7. The validity of the level of theory was supported by the agreement between structural parameters of the solid-state structure, as determined by XRD, and the calculated model for complex **4**, as can be seen in Table S8 and Figure S47, which shows an overlap of the two structures.

Isosurface plots of the selected frontier molecular orbitals are shown in Figure 5 (for complexes **2** and **5**) and Figures S48–S53. The HOMO in complexes **1** and **2** had contributions from the Pt center and also the

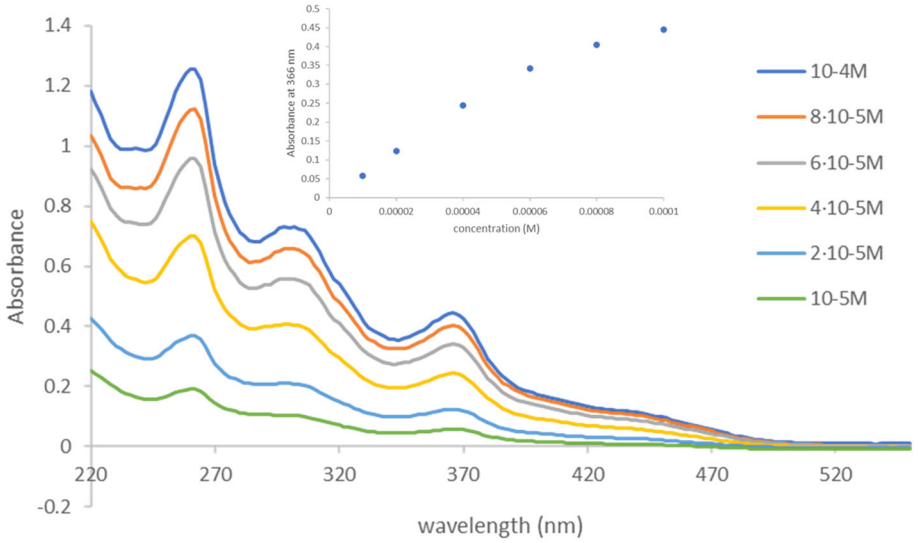

FIGURE 4 UV–vis absorption spectra of complex **5** in degassed acetonitrile at different concentrations. Inset: representation of absorption against concentration at $\lambda = 366$ nm.

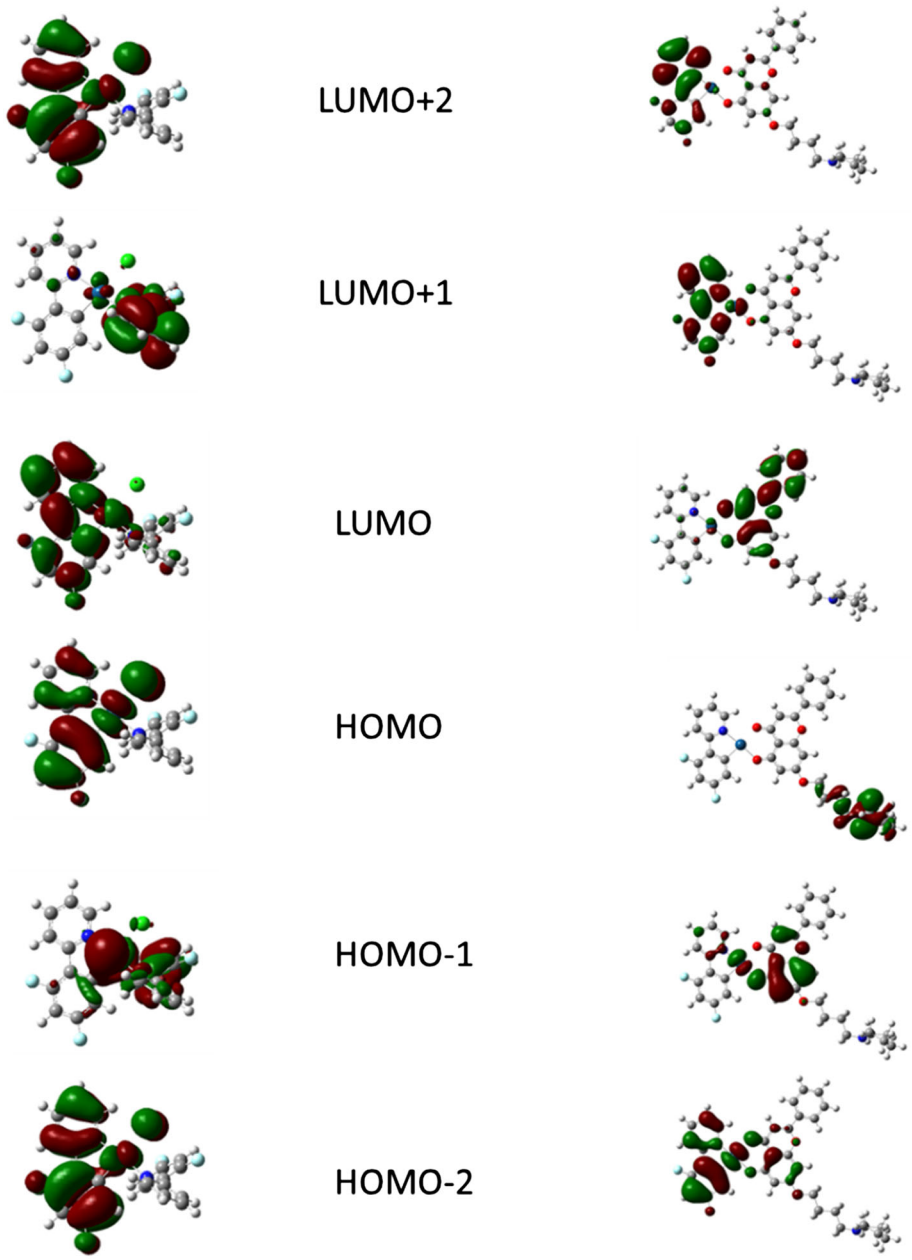

FIGURE 5 Schematic representation of the frontier orbitals of complex **2** (left) and **5** (right).

cyclometalating and chloride ligands (see Table S6). Several differences were observed in the percentage values, with a higher participation of the Pt orbitals for **2** and those of the C^N ligand for **1**. The influence of the ancillary ligand on the percentage of Pt 5d orbital character that contributes to the HOMOs was reported previously.[82] The LUMOs in these complexes had the same energy and were mainly centered over the cyclometalated ligand, with contributions around 86%–88%. The HOMO was more stabilized in **2**, and this is almost certainly due to the presence of the fluoro-substituents in the dfppy ligand, which increase the HOMO–LUMO gap.

The substitution of the monodentate N-donor ligand in **1** and **2** by PTA (complexes **3** and **4**) led to stabilization of the orbitals, which involve the participation of the chelating C^N ligands and the Pt atom (Figure 6). The orbitals that were mainly contributed by the PTA ligand appeared at the same energy in both complexes, but in the case of **3**, these orbitals were more stabilized than the orbital analogous to the HOMO of **1** while in **4**, they were of higher energy. In fact, in complex **4**, one of the orbitals contributed by PTA was the HOMO and that analogous to the HOMO of **2** was HOMO-2 (Figure 6 and Table S6). The LUMOs of these complexes were of similar energy and were also mainly centered over the cyclometalated

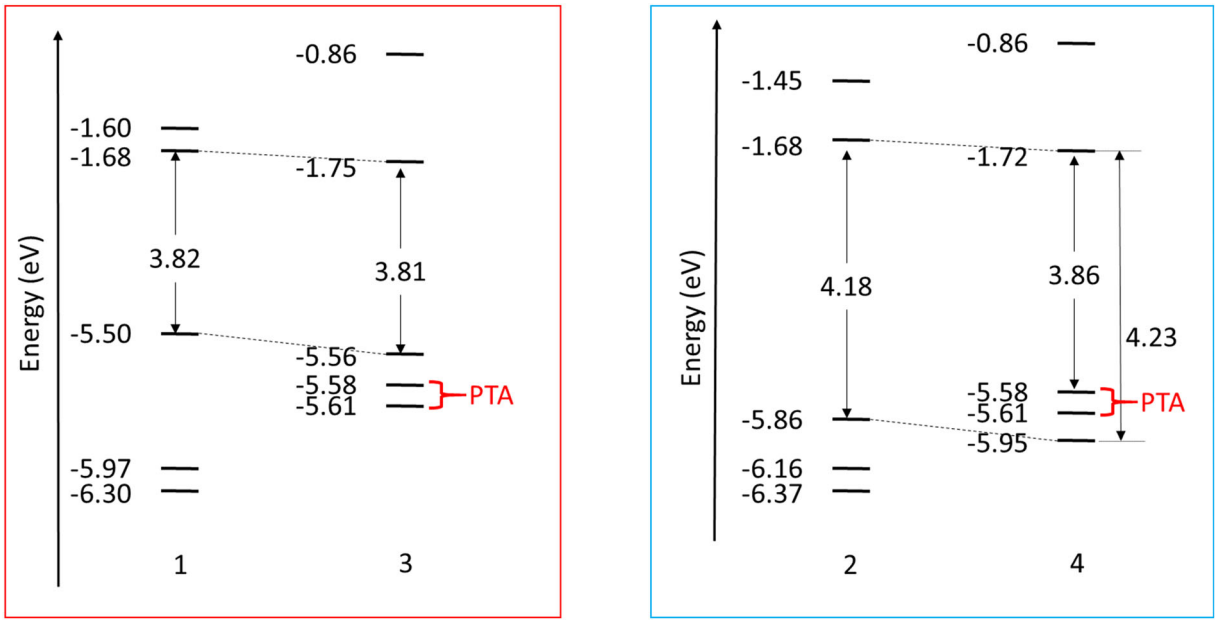

FIGURE 6 Energies (eV) of the main molecular orbitals of complexes **1**–**4**.

ligand, with contributions around 85%. The frontier orbitals of **1**–**3** were similar to analogous orbitals described for other [Pt(C^N)X(L)] complexes.[7,18] However, the situation found in **4** is unprecedented in these kinds of complexes with phosphane ligands, and DFT calculations for platinum cyclometalated complexes containing a PTA ligand have not been reported to date.

In complexes **5** and **6**, the frontier molecular orbitals are very similar and markedly different to those of the other complexes. In these cases, the HOMO was located over the aliphatic chain and its terminal piperidine (or morpholine) ring; and for HOMO-1, although there is some participation of the Pt center, the main contribution came from the chrysin ligand, especially Ring A. The orbital in which the Pt atom and the C^N ligand participated was HOMO-2. The LUMO was spread over the chrysin fragment and was mainly located in rings C and B. Thus, the introduction of the chrysin ligand led to a dramatic modification of the frontier orbitals with respect those of the dfppy complexes **2** and **4**.

TD-DFT calculations were carried out to elucidate the nature of the low-lying singlet and triplet states at the geometries of the ground state (see Tables S6 and S7). In complexes **1**–**3** the S_1 state had a contribution from a HOMO to LUMO transition. In complex **4**, however, S_1 and S_2, which involve the HOMO and HOMO-1 orbitals participated by PTA, had a negligible oscillator strength, and the experimental transition should correspond to S_3, which mainly corresponds to the HOMO-2 to LUMO transition. In the four complexes, the transition supported a mixed ^{1}MLCT (Pt to C^N), ^{1}LC (C^N), and ^{1}LLCT (small participation, Cl to C^N in **1**, **2**, and **4** and PTA to C^N in **3**) charge transfer character. In complexes **1** and **3**—containing the thpy ligand—the contribution from the ^{1}LC transition was more important while in **2** and **4**, the contributions of ^{1}MLCT and ^{1}LC were quite similar. It is interesting to note the similarities between the theoretical values (Table S6) for the transitions of **1** and **3**, on the one hand, and **2** and **4** on the other. Higher energies were obtained in the case of the dfppy complexes, and this is in good agreement with the experimental spectra.

The situation was different for complexes **5** and **6**, and the ligand that participated in the transitions was the chrysin **L1** (**5**) or **L2** (**6**) and not the cyclometalated dfppy. The S_1 state was contributed by a HOMO-1 to LUMO transition supporting a mixed ^{1}LC (**L**, 71%) and ^{1}MLCT (Pt to **L**, 24%) (similar in both complexes) charge transfer character. Closer inspection of the orbitals involved (see above) showed that the main character of the transition can be assigned to a transfer from Ring A to Rings B and C on the chrysin ligand. The HOMO that had a contribution from the chrysin ligand, but only in the lateral chain, did not participate in the transition.

As found for the S_1 states, the T_1 states in complexes **1**–**3** were mainly defined by transitions from the HOMO to the LUMO, while in **4**, the transition was from the HOMO-2 to the LUMO. Once again, the HOMO and HOMO-1 orbitals that mainly involved the PTA ligand did not participate. The aforementioned transitions can be described as ^{3}MLCT (Pt to C^N) along with ^{3}LLCT

(Cl to C^N in **1**, **2**, and **4** and PTA to C^N in **3**) and ^{3}LC (C^N to C^N) triplets. The ^{3}LC component was higher for **1** and **3**, and this is consistent with the fact that the structure of the bands was more clearly observed and with the lower effect of the solvent polarity in comparison with **2** and **4** (Figures S39c–S42c).

In the case of complexes **5** and **6** the calculated T_1 was mainly defined by a transition from the HOMO-1 to the LUMO, and this can be described mainly as ^{3}LC (**L1** to **L1** for **5** or **L2** to **L2** for **6**) but also as ^{3}MLCT (Pt to **L**). It is noteworthy that, apart from the metal center, the orbitals that participate in the transition were those of the chrysin ligand and not those of the dfppy ligand. The behavior of complexes **5** and **6** was clearly different from the other complexes, and this highlights the strong influence of the ancillary **L1** or **L2** ligands.

To the best of our knowledge, DFT analysis of a cyclometalated Pt complex with a relatively similar O^O ligand has not been published to date. The molecular orbitals and transitions reported for different [Pt(C^N)(acac)] (or substituted acac) complexes[82,88–90] are not comparable, and they do not reflect such a strong participation of the O^O ligand as that found in **5** or **6**. It is necessary to consider that, in contrast to the situation for **L1** or **L2**, in the acac complexes, both oxygen atoms are equivalent. In the case of [Pt(ppy)(8-Q)] (8Q = 8-quinolinate), which is a three-electron ligand like **L1** or **L2**, the S_1 and T_1 states involve a HOMO to LUMO transition that mainly affects the electron density on the 8-Q ligand (phenolate to pyridine LC on the 8-Q ligand) although the transitions do carry some contribution of a Pt-ppy MLCT admixture.[91] This case is more similar to the behavior of **5** or **6**, although for [Pt(ppy)(8-Q)], the HOMO and LUMO exhibit some degree of participation from the orbitals of the ppy ligand.

The geometries of the lowest triplet state (T_1) of complexes **1**–**6** were optimized using the spin-unrestricted DFT approach. After this geometry relaxation, the difference in energy of each T_1 state with its related S_0 was calculated (adiabatic energy differences). The higher experimental energy values for the dfppy complexes **2** and **4**, as compared with the thpy derivatives **1** and **3**, are consistent with the sequence observed in the theoretical values. The calculated energies of **1** and **3** were very similar to those obtained experimentally, although in **2** and **4** they were somewhat underestimated. Complexes **5** and **6** are a case apart in that, although there are dfppy complexes, both the experimental and theoretical energy values were low—although they were overestimated in the calculations (Table S9).

The spin-density distribution in the optimized T_1 states of these complexes supports the conclusions drawn from the TD-DFT calculations for the T_1 states. For complexes **1**–**4**, the spin-density distribution in the optimized T_1 state was spread over the cyclometalated ligand, with a small contribution from the metal center (see Table S10, Figures 7 and S54). However, in complexes **5** and **6**, the participation in the spin-density of the ortho-metalated ligand was very low and the main contribution was in the oxygen-donor chelating ligand (see Table S10), with a small participation of the platinum center.

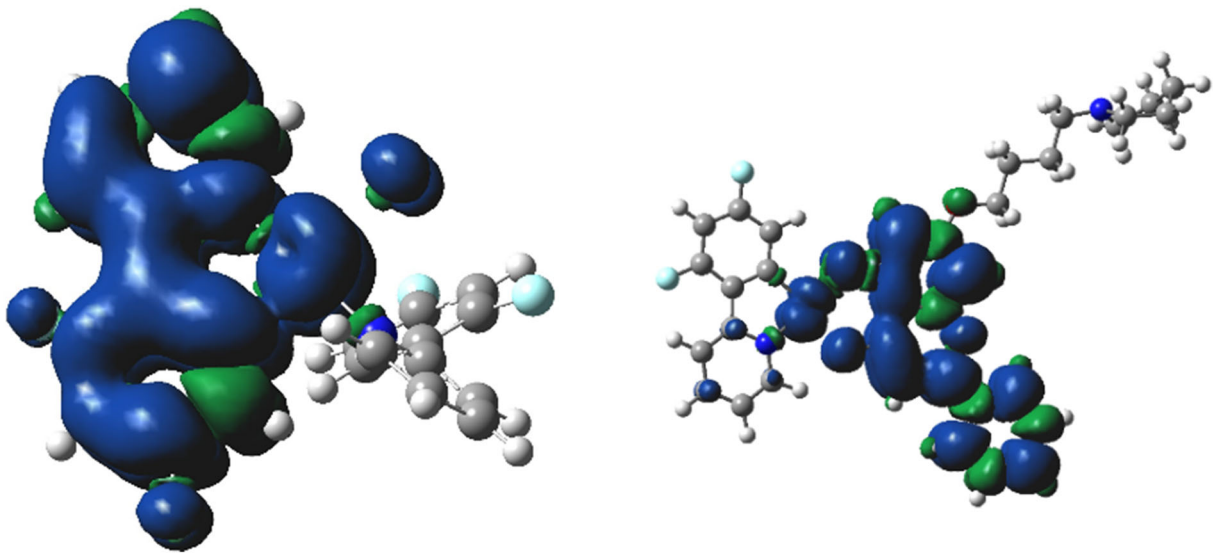

FIGURE 7 Calculated spin density distribution for complexes **2** (a) and **5** (b).

3.5 | Speciation of 1, 2, and 5 in DMSO and DMSO/H_2O

In the biological studies (see below), the complexes were initially dissolved in DMSO and then in water to prepare the solutions to be applied to the cell culture medium. As a consequence, the possible evolution in these solvents of the most cytotoxic complexes (**1**, **2**, and **5**, see below) was studied. The study was performed by ^{1}H NMR and UV–vis spectroscopy. The ^{1}H NMR analysis was mainly performed by monitoring the H^6 resonances of the pyridine ring. These signals are easily distinguished by $^3J_{HH}$, which has a value of around 5–6 Hz,[77,92] that is, smaller than the coupling observed for other protons of the aromatic rings. Furthermore, ^{195}Pt satellites were observed in some cases for these signals.

3.5.1 | Evolution in DMSO

In the case of **1**, 2 h after the addition of DMSO-d_6 very small resonances due to the free ligand Hthpy were observed and a new product **1a** appeared, with signals of the same intensity for both products (see Figure 8). We propose that this new product is the solvated species [Pt(thpy)Cl(DMSO)], in which one molecule of DMSO has displaced the Hthpy ligand coordinated only by the pyridine ring. After 24 h, complex **1** was the major species in solution (the **1**:**1a** ratio was 76:24). When the solution was left to stand for 48 h this ratio was 52:48.

In the case of **2**, on addition of DMSO-d_6 small resonances for the free ligand Hdfppy appeared and a new product, **2a**, was formed (see Figure S55). In a similar way to the case of **1**, we propose that this new product is the solvated species [Pt(dfppy)Cl(DMSO)]. After 24 h, the complex **2**:**2a** ratio was 47:53, and at 48 h, it was 19:81, thus showing a higher degree of evolution in **2** than in **1**. This difference could be due to a higher *cis* effect of the orthometalated ring in **2**, which is more π-electron withdrawing. Coincidentally, **2** is more cytotoxic than **1** (see below).

In the DMSO-d_6 solution of **5** (Figures S56–S57), the formation of a new product, **5a**, was barely evident after 1 h. After 24 h, however, the **5**:**5a** ratio was 65:35, and after 48 h, it was 50:50. Very small resonances due to

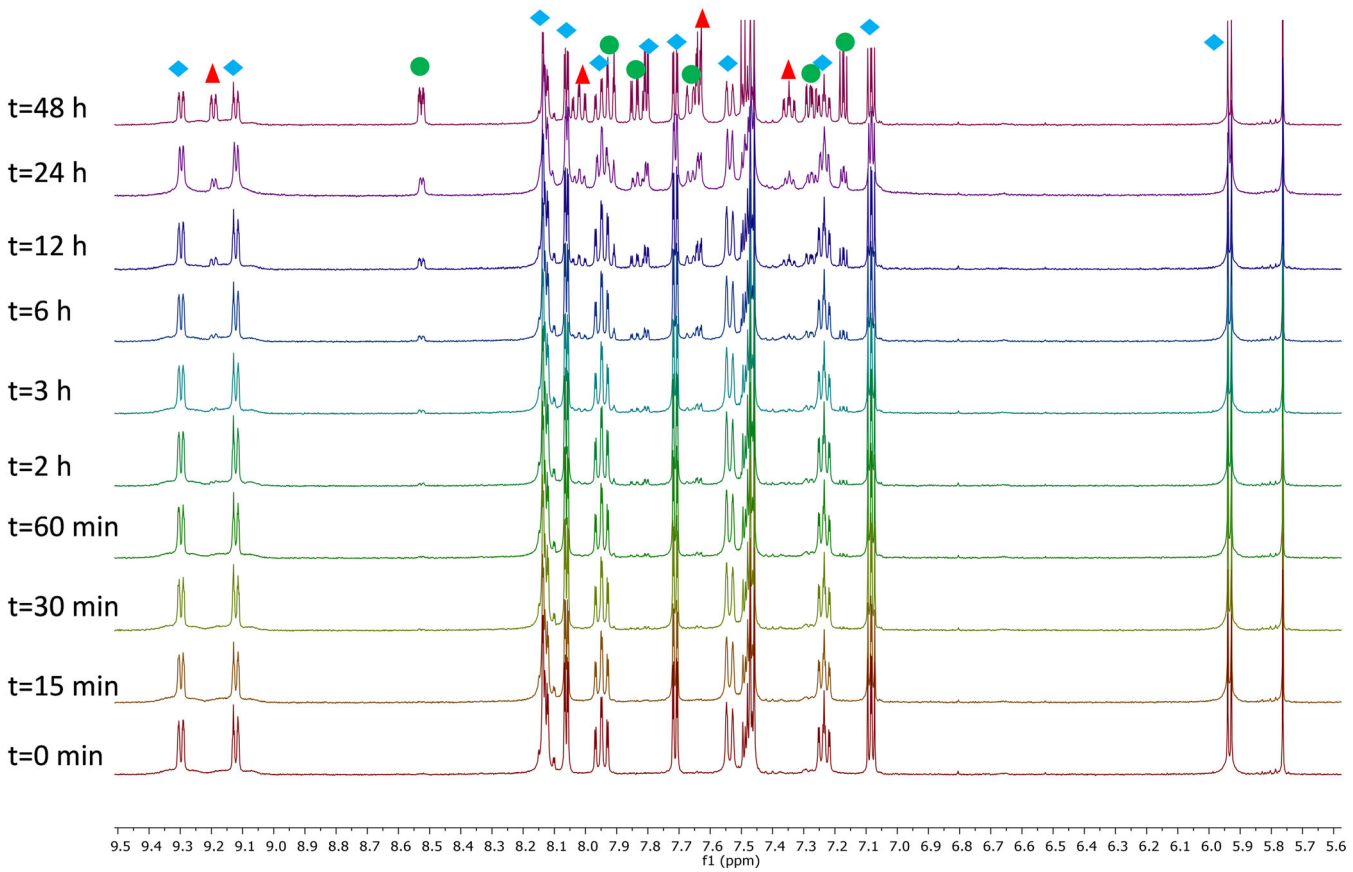

FIGURE 8 ^{1}H nuclear magnetic resonance (NMR) monitoring of the evolution of complex **1** in dimethylsulfoxide (DMSO)-d_6. Blue diamonds = **1**, red triangles = **1a**, green circles = Hthpy.

HL1 were observed (11% and 12% at 24 and 48 h, respectively). Concerning the composition of **5a**, several facts must be taken into account: (i) this compound contains a dfppy ligand with resonances similar to those of **5**; (ii) **5a** contains a deprotonated chrysin ligand; (iii) the resonances of Ring A of **L1** are very similar to those of **5** (6.50 and 6.54 ppm in **5** and 6.58 ppm in **5a**) while a more marked difference is found in the singlet of Ring C (7.48 ppm in **5** and 7.33 ppm in **5a**). We therefore propose that the stoichiometry of **5a** is [Pt(dfppy)(κ^1-L1)(DMSO)] with **L1** coordinated only by the anionic oxygen atom. This kind of di- to mono-coordinated evolution after solvolysis has been proposed, based on the results of computational studies, for a 3-aminoflavone coordinated to a "$Pt(PMe_3)_2$" fragment.[49]

3.5.2 | Evolution in water

The complexes were not sufficiently soluble in D_2O to obtain an NMR spectrum, and as a consequence, the study of the evolution in the presence of water was carried out in DMSO-d_6/D_2O mixtures. The amount of D_2O used was the maximum possible that allowed the solubilization of the complexes to register the ^{1}H NMR spectra.

In the cases of **1** or **2**, dissolved in a DMSO-d_6/D_2O (90:10) mixture, the evolution was similar to that observed in neat DMSO-d_6 (Figures S58–S59). However, the rate of formation of **1a** or **2a** in the mixture was slower compared with that observed in DMSO-d_6 alone. In fact, signals for **1a** only became visible after 6 h and the **1**:**1a** ratio after 48 h was 61:39. The **2**:**2a** ratio in the mixture of solvents after 48 h was 43:57. The evolution of **2** was also faster than that of **1** under these conditions. The decrease in the rate of the evolution to **1a** or **2a** in the presence of water led us to propose that in this mixture, the same DMSO adducts were formed and the process is dependent on the DMSO concentration. Furthermore, the chemical shifts of the species formed in both cases are very similar, even with a certain change in the solvent. Another fact to support this proposal is that a crystal of **2a** (see above for the description of the structure determined by X-ray diffraction) was formed in an NMR tube containing a solution of **2** in the DMSO-d_6/D_2O mixture. The evolution of **1** and **2** was also studied by UV–vis spectroscopy in a mixture with a higher percentage of H_2O (DMSO:H_2O = 43:57 for **1** and 40:60 for **2**) and a transformation was also observed, presumably corresponding to the formation of **1a** or **2a** although the formation of water adducts cannot be completely discarded (Figures S60–S61).

A solution of **5** in a DMSO-d_6/D_2O (95:5) mixture led to the formation of a larger amount of **HL1** than in DMSO-d_6 alone. **HL1** should be formed by protonation of **L1** in the complex. The presence of increasing amounts of **5a** was also observed (Figures S62–63). The formation of a precipitate was observed and this could correspond to hydroxo-platinum species.[93] Hydroxo-platinum complexes have been proposed as evolution products from cisplatin.[94] The evolution with time of the three species detected in solution is represented in Figure S64. It is noteworthy that the amount of **HL1** increased up to three hours and thereafter only small changes were observed. It is possible that the increase in pH that should lead to protonation of **L1** could slow down the formation of **HL1**. For the sake of comparison, the evolution products of **5** after 48 h in DMSO or in a DMSO/D_2O (95:5) mixture is shown Figure S65. It was observed that a higher amount of **5a** was formed when D_2O was present.

The evolution of **5** in a DMSO/H_2O mixture (80:20) was also monitored by UV–vis spectroscopy. The changes observed at 272 nm, that is, the region in which **HL1** absorbs, were relatively complex, but the formation of a new product was detected by the presence of a band at around 332 nm (see Figure S66).

In conclusion, for complexes **1** and **2** in DMSO, solvolysis, which started after several hours, was slowed down in the presence of water and led to the adducts [Pt(C^N)Cl(DMSO)]. In the case of **5**, the formation in DMSO of [Pt(dfppy)(κ^1-L1)(DMSO)] was monitored, and when D_2O was present, ligand **HL1** was also detected.

3.6 | Biological studies

3.6.1 | Cytotoxic and photocytotoxic activity

The anticancer potential of complexes **1**–**5** was evaluated along with the biological mechanism of action. First, the cytotoxic activity of the complexes towards HeLa human cervical cancer cells was ascertained by MTT assays. Cells were cultivated with different concentrations of the complexes (from 0 to 50 μM) for 48 h to determine the concentration required to inhibit cell viability by 50% (IC_{50}) (Table 3). Cisplatin was included in the experiment as a chemotherapeutic drug reference. The IC_{50} values obtained were 18.82 ± 2.93 μM for **1**, 10.80 ± 1.54 μM for **2**, and 31.50 ± 5.80 μM for **5**. Interestingly, the IC_{50} value of complex **2** is similar to that of cisplatin under the same conditions (7.78 ± 0.07 μM). In contrast, complexes **3** and **4** displayed IC_{50} values > 50 μM and were considered non-active against cancer cells. The antineoplastic activity of complexes **1**, **2**, and **5** was further evaluated against a lung adenocarcinoma cell line (A549) (Table 3). Once again, complex **2** displayed the highest cytotoxicity, with

TABLE 3 Cytotoxic and photocytotoxic activity

	HeLa			A549		
	IC_{50} (μM)			IC_{50} (μM)		
Cell line	Dark	Light	PI	Dark	Light	PI
1	18.82 ± 2.93	6.62 ± 1.11	2.84	28.97 ± 2.98	21.76 ± 6.84	1.33
2	10.80 ± 1.54	7.11 ± 1.96	1.52	20.67 ± 0.73	18.64 ± 7.99	1.15
5	31.50 ± 5.80	24.05 ± 1.43	1.31	30.81 ± 2.95	26.81 ± 5.23	1.15
Cisplatin	7.78 ± 0.07			10.40 ± 0.34		

Note: Cells were treated with the complexes under dark conditions or irradiated with a blue light (1 h, 150 mW/cm^2, λ: 460 nm) after 4 h of pretreatment. IC_{50} values were determined 48 h later by an MTT assay. Data represent the mean ± *SD* of at least two independent experiments, each performed in triplicate. PI, phototoxicity index = $IC_{50,dark}/IC_{50,light}$.

an IC_{50} of 20.67 ± 0.73 μM, while the IC_{50} of complexes **1** and **5** were 28.97 ± 2.98 μM and 30.81 ± 2.95 μM, respectively. These values are two to three times higher than that of cisplatin (10.40 ± 0.34 μM) in A549 cells, which indicates that the complexes might have a lower cytotoxic effectiveness against lung adenocarcinomas. Overall, these results show that compound **2** has the greatest potential as an antineoplastic agent.

The potential of the complexes as photosensitizers for PDT was also explored. Different Pt (IV) compounds that are photoactivated by a PACT (photoactivated chemotherapy) mechanism to render Pt (II) cytotoxic agents have been described,[95] but very few Pt (II) compounds have been shown to exhibit photosensitizing effects via a PDT mechanism. Pt-porphyrin[96,97] or Pt-BODIPY[98] derivatives and also two cyclometalated derivatives[12,99] have been reported as PDT agents. To determine the potential photodynamic activity of our complexes, HeLa and A549 cancer cells were incubated with different concentrations of **1**, **2**, and **5** for 4 h to allow their cellular internalization. The complexes were then photoactivated for 1 h with a blue light (λ_{ir} = 460 nm). A total light dose of 24.1 J cm^{-2} was delivered, which is within the range of doses applied for the photoactivation of other metal complexes.[95] In HeLa cells, the cytotoxicity of **1** increased moderately following irradiation to give a photocytotoxicity index (PI) ($IC_{50\ dark}/IC_{50\ light}$) of 2.84. The resulting $IC_{50\ light}$ value was similar to that of cisplatin in the dark, thus revealing that the complex would have a highly effective cytotoxic capacity after photoactivation. In contrast, the activities of complexes **2** and **5** against HeLa cells were only slightly modified by photoactivation, with PI values <2. In A549 cells, none of the complexes showed photodynamic behavior (PI < 2). Overall, these data reveal that only complex **1** exhibits moderate photosensitizing properties and these seem to be cancer-type specific. Apparently, the ^{3}LC nature of T_1 in **5** is not suitable for appropriate photoactivation. As far as **1** and **2** are concerned, both of which have a T_1 of ^{3}MLCT and ^{3}LLCT nature, the low photoactivation of **2** may be due to a small molar extinction coefficient at 460 nm. In fact, excluding **5**, complex **1** exhibits the highest molar absorption at the wavelength used in the biological experiments.

The hemolytic activities of complexes **1**, **2**, and **5** were explored in order to rule out any toxicity on healthy erythrocytes through cellular membrane damage. To this end, freshly isolated porcine RBCs were treated with the complexes at different concentrations and the hemoglobin release, as a consequence of the membrane rupture, was measured. As a positive control, RBCs were exposed to a solution of 2% Triton X-1000 to achieve the maximal hemoglobin release. Importantly, none of the three complexes exhibited hemolytic activity (hemolysis <5% compared with positive control) at concentrations up to 50 μM (Table S11), which is higher than the IC_{50} values of the complexes in cancer cells. These results show that the compounds have good blood compatibility at the chemotherapeutic dose.

3.6.2 | Cellular localization and damage

The type of cell damage generated by metal-based complexes depends largely on their location within the cells. To explore the cellular distribution of complexes **1**, **2**, and **5**, cells were incubated with the complexes at 25 μM, and 3 h later, their localization was examined by confocal microscopy. An excitation wavelength (λ_{ex}) of 405 nm was applied, and the fluorescence emission was determined at different wavelengths (λ_{em}) (450, 525, and 595 nm). Fluorescence was not detected in cells treated with **1** and **2**, probably as a consequence of their low absorption at 405 nm (See Figures S67–S68). In contrast, in cells exposed to complex **5**, a bright fluorescence emission was observed at 595 nm (Figure S69). High

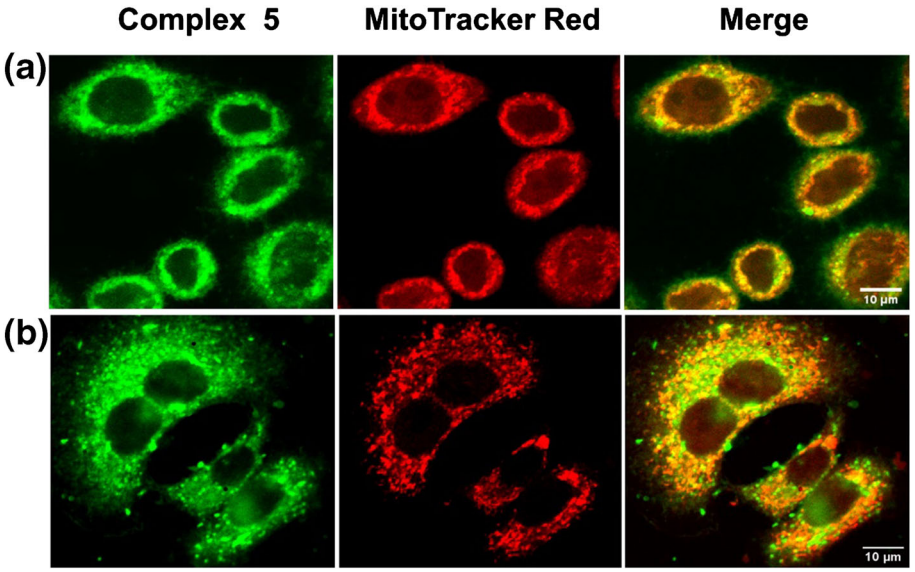

FIGURE 9 Confocal microscopic imaging of the subcellular localization of complex **5**. HeLa (a) and A549 (b) cells were incubated with the complex at 25 μM for 1 h at 37°C. Mitochondria were stained with MitoTracker Red™. The localization of the complex is indicated by the green fluorescence (λ_{ex}: 488 nm; λ_{em}: 595 nm). Mitochondria staining is shown by the red fluorescence (λ_{ex}: 488 nm; λ_{em}: 595 nm). Colocalization can be observed in yellow in the merged images.

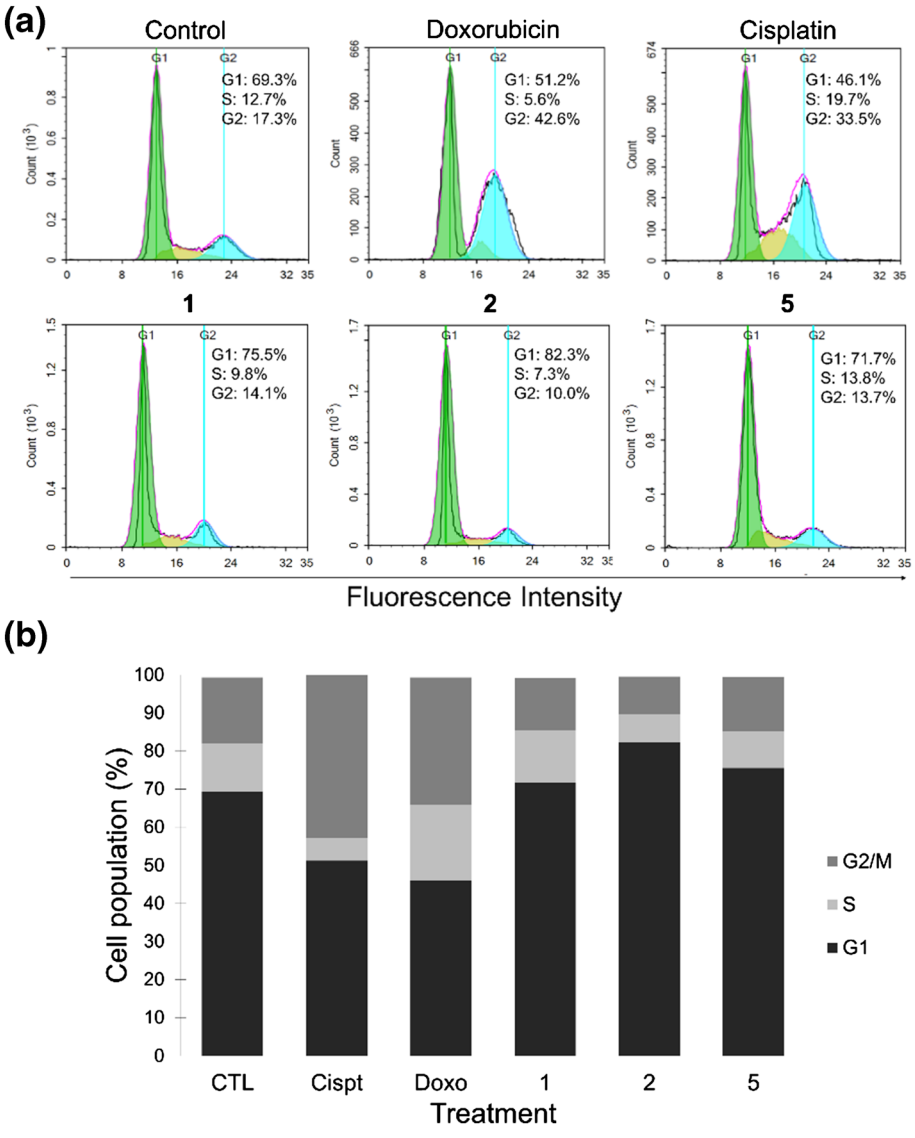

FIGURE 10 Effect of complexes **1**, **2**, and **5** on cell cycle distribution. A549 cells were treated for 24 h with medium alone as a control, cisplatin (Cispt) (5 μM), doxorubicin (Doxo) (0.5 μM), or complexes **1**, **2**, and **5** at the corresponding IC_{50}. (a) Representative flow cytometry histograms of cell cycle distribution of propidium iodide-stained cells. The percentage of cells in G1, S, and G2/M phases are indicated. (b) Stacked bar graphs showing the percentage of cells in each phase of the cell cycle.

magnification images of HeLa and A549 cells revealed a punctate fluorescence pattern throughout the cytoplasm, which suggests that complex **5** is mostly localized in vesicular organelles (Figure 9). In contrast, fluorescent particles were not detected in the cell nucleus. Co-staining of the cells with a fluorescent probe for mitochondria (MitoTracker Red™) revealed that **5** notably colocalizes with mitochondria, as seen in yellow in the merged image (Figure 9). The Manders overlap coefficient measured between complex **5** and MitoTracker Red™ was 0.74 in HeLa cells and 0.63 in A549 cells, thus corroborating a significant accumulation of the complex in mitochondria.

The cellular damage exerted by chemotherapeutic drugs, for example, cisplatin and doxorubicin, is mediated mainly by their interaction with genomic DNA, which triggers a cellular response that culminates in the activation of apoptosis. However, given that the intracellular distribution of complex **5** was restricted to the cytoplasm, it is likely that the cytotoxic effect induced by complexes **1**, **2**, and **5** involves an alternative mechanism of action to DNA damage. This was investigated by comparing the effect of the complexes on cell cycle to that of cisplatin and doxorubicin. To this end, after 24 h of treatment with the complexes at the corresponding IC_{50}, A549 cells were stained with PI, a red-fluorescent DNA intercalator, and the DNA content was examined by flow cytometry. It has been reported that the interaction of cisplatin with DNA induces a transient cell cycle arrest in S phase followed by a durable G2/M arrest.[100] Similarly, doxorubicin exerts an antiproliferative effect through cell cycle arrest at the G2/M phase.[101] As expected, an increase in the proportion of cells in S and in G2/M phases was detected in cells exposed to cisplatin (19.7% in S and 33.5% in G2/M) and in the G2/M phase (42.6%) after doxorubicin treatment in comparison with control untreated cells (12.7% in S and 17.3% in G2/M) (Figure 10). In contrast, a very modest effect on the cell cycle progression was observed in cells treated with complexes **1**, **2**, and **5**. Overall, these results confirm that the cytotoxic effect of the complexes is generated by an alternative molecular mechanism to that of nuclear DNA-damaging chemotherapeutic agents, which would involve cellular targets outside the nucleus.

Mitochondria are organelles that control essential cell functions and regulate apoptotic cell death. Importantly, mitochondria exert central bioenergetic and metabolic functions that provide energy and anabolites, which in cancer cells are crucial for tumor growth.[102] Thus, mitochondria constitute promising targets for the development of novel anticancer agents. Several Pt (II) complexes capable of promoting cell apoptosis by affecting mitochondrial functions have been described.[103,104] Thanks to the electron chain transport complexes and ATP synthase located in the inner mitochondrial membrane, mitochondria supply the cell with energy in the form of ATP from the metabolic oxidation of substrates. Maintaining stable levels of intracellular ATP is crucial for normal cell functioning. The high degree of colocalization of complex **5** in mitochondria prompted us to analyze the capability of the complexes to induce mitochondrial damage by determining their effect on ATP production. The ATP content of the cells was assessed with the CellTiter-Glo® Luminescent reagent, which generates a luminescent signal proportional to the amount of ATP present. It was found that the cellular ATP levels decreased significantly by 36.6 + 1.8%, 36.7 + 4.0%, and 17.0 + 6.4% after treatment with **1**, **2**, and **5**, respectively, at the corresponding IC_{50} in comparison with control untreated cells (Figure 11). Overall, these results point to mitochondria as the principal intracellular target for the cytotoxic activity of these complexes.

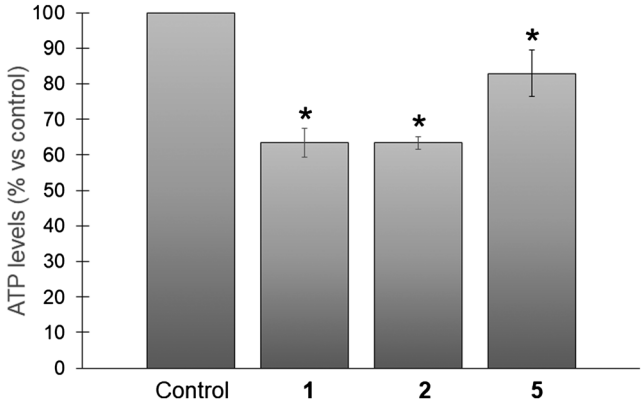

FIGURE 11 Effect of complexes on adenosine triphosphate (ATP) production. A549 cells were incubated for 4 h at 36°C with complexes **1**, **2**, and **5** at the corresponding IC_{50} or with medium alone as a control. ATP content was measured by adding CellTiter-Glo® Reagent and recording the luminescence of each sample. Data shown represent the percentage versus untreated control cells (mean ± *SD*; $n = 4$). *$p < 0.05$ versus control cells.

4 | CONCLUSIONS

A series of cyclometalated (2-[2′-thienyl]pyridinate, thpy, and 2-[2,4-difluorophenyl]pyridinate, dfppy) platinum complexes with N-donor, PTA, or chrysin-derived ligands (incorporating piperidine, **HL1**, or morpholine, **HL2**, fragments) was prepared. The influence that the cyclometalated and ancillary ligands have on the photophysical

and anticancer properties has been demonstrated. The solid-state structures of [Pt(dfppy)Cl(PTA)] and [Pt(dfppy)Cl (DMSO)] were solved by X-ray diffraction. Luminescence studies showed that the complexes exhibit a phosphorescent or fluorescence character (lifetimes in the range 2.069–1658 ns) with tunable emission wavelengths between 393 and 616 nm and quantum yields up to 6.8%. Aggregation phenomena in solution were found for complex **5**. Supporting TD-DFT studies were performed and demonstrated the differentiating characteristics of the MOs of [Pt(dfppy)L], (L = **L1**, **5**; L = **L2**, **6**) complexes, with a strong participation of the chrysin ligand. For the complexes with N-donor or PTA ligands (**1**–**4**) the contribution of the Pt(5d) and C^N orbitals to the calculated HOMO was ligand-dependent, while the LUMOs were in general localized over the C^N ligands. TD-DFT calculations showed that, in the cases of complexes **1**–**4**, the S_1 and T_1 states reflect mainly MLCT (Pt to C^N) and LC (C^N) contributions, with a higher participation of the LC transition for the thpy derivatives. The situation is completely different in the case of the chrysin derivatives **5** and **6**. In these compounds the main contribution to S_1 and T_1 states comes from an LC transition that involves an electron redistribution in the **L1** or **L2** ligand, without the participation of the C^N ligand. Complexes **1** and **2** evolve to $[Pt(C^N)Cl(DMSO)]^+$ in DMSO or DMSO/water (90:10), and in the case of **5**, the formation in DMSO of [Pt(dfppy)(κ^1-L1)(DMSO)] was monitored, and when D_2O was present, **HL1** was also detected.

Biological studies showed that of the different cyclometalated platinum complexes, complexes **1**, **2**, and **5** exert cytotoxic activity against human cervical (HeLa) and lung (A549) carcinoma cells. The best IC_{50} values were obtained for compound **2** (10.80 ± 1.54 μM in HeLa cells and 20.67 ± 0.73 μM in A549 cells). Interestingly, the activity of complex **1** increased after irradiation with blue light, with a photocytotoxicity index of 2.84 obtained. Microscopy assays on complex **5**, which exhibited luminescent properties that could be exploited in imaging techniques, revealed that this complex is localized outside the cell nucleus—mainly in the mitochondria. This finding was supported by analysis of the cell cycle progression of the cells, where it was observed that the mechanism of action of the complexes is different from that of other chemotherapeutic agents such as cisplatin and doxorubicin, which interact with nuclear DNA. Our results suggest that the activity of the complexes at the mitochondrial level, which notably reduced the cellular ATP content, would be highly relevant to their anticancer activity because interference with mitochondrial metabolism has been shown to have a major impact on tumor progression.

The results of this study illustrate how the choice of specific ligands around the metal center can have a dramatic impact on the orbital configuration and the photophysical and cytotoxic properties. The influence of the chrysin ligand on the MOs of the corresponding complex pave the way to modifications of this ligand to tune the properties. Furthermore, the cyclometalated platinum complexes developed in this project, in particular complex **2**, could provide an alternative cytotoxic chemotherapeutic mechanism that is of great interest for the treatment of tumors with resistance to current anticancer drugs. In any case, modifications to the structure would be of interest to increase the cytotoxic activity.

ACKNOWLEDGMENTS

We acknowledge the financial support provided by the Spanish Ministerio de Ciencia, Innovación y Universidades (MCIU), Agencia Estatal de Investigación (AEI), and Fondo Europeo de Desarrollo Regional (FEDER) (RTI2018-100709-B-C21 to B. R. M., RTI2018-100709-B-C22 to A. M.), Junta de Comunidades de Castilla-La Mancha-FEDER (JCCM) (grant SBPLY/19/180501/000260 to B. R. M.) as well as UCLM-FEDER (grants 2020-GRIN-29093 and 2021-GRIN-30981 to F. A. J.). G. D. thanks the Junta de Comunidades de Castilla la Mancha and EU for financial support through the European Regional Development Fund (project SBPLY/19/180501/000191). E. Z. acknowledges the Generalitat de Catalunya (AGAUR; 2021 FI_B 01036) for a predoctoral fellowship.

REFERENCES

[1] J. A. G. Williams, S. Develay, D. L. Rochester, L. Murphy, *Coord. Chem. Rev.* **2008**, *252*, 2596.
[2] J. R. Berenguer, E. Lalinde, M. T. Moreno, *Coord. Chem. Rev.* **2018**, *366*, 69.
[3] J. Kalinowski, V. Fattori, M. Cocchi, J. A. G. Williams, *Coord. Chem. Rev.* **2011**, *255*, 2401.
[4] Á. Díez, E. Lalinde, M. T. Moreno, *Coord. Chem. Rev.* **2011**, *255*, 2426.
[5] N. Cutillas, G. S. Yellol, C. De Haro, C. Vicente, V. Rodríguez, J. Ruiz, *Coord. Chem. Rev.* **2013**, *257*, 2784.
[6] J. R. Berenguer, J. G. Pichel, N. Giménez, E. Lalinde, M. T. Moreno, S. Piñeiro-Hermida, *Dalton Trans.* **2015**, *44*, 18839.
[7] A. I. Solomatina, P. S. Chelushkin, D. V. Krupenya, I. S. Podkorytov, T. O. Artamonova, V. V. Sizov, A. S. Melnikov, V. V. Gurzhiy, E. I. Koshel, V. I. Shcheslavskiy, S. P. Tunik, *Bioconjug. Chem.* **2017**, *28*, 426.
[8] M. Jamshidi, M. Babaghasabha, H. R. Shahsavari, S. M. Nabavizadeh, *Dalton Trans.* **2017**, *46*, 15919.
[9] A. Bossi, A. F. Rausch, M. J. Leitl, R. Czerwieniec, M. T. Whited, P. I. Djurovich, H. Yersin, M. E. Thompson, *Inorg. Chem.* **2013**, *52*, 12403.

[10] K. Li, G. S. M. Tong, J. Yuan, C. Ma, L. Du, C. Yang, W. M. Kwok, D. L. Phillips, C. M. Che, *Inorg. Chem.* **2020**, *59*, 14654.

[11] T. Okada, I. M. El-Mehasseb, M. Kodaka, T. Tomohiro, K. Okamoto, H. Okuno, *J. Med. Chem.* **2001**, *44*, 4661.

[12] S. W. Lai, Y. Liu, D. Zhang, B. Wang, C. N. Lok, C. M. Che, M. Selke, *Photochem. Photobiol.* **2010**, *86*, 1414.

[13] R. W. Y. Sun, A. L. F. Chow, X. H. Li, J. J. Yan, S. S. Y. Chui, C. M. Che, *Chem. Sci.* **2011**, *2*, 728.

[14] A. Zamora, S. A. Pérez, M. Rothemund, V. Rodríguez, R. Schobert, C. Janiak, J. Ruiz, *Chem. - a Eur. J.* **2017**, *23*, 5614.

[15] R. Cortés, M. Tarrado-Castellarnau, D. Talancón, C. López, W. Link, D. Ruiz, J. J. Centelles, J. Quirante, M. Cascante, *Metallomics* **2014**, *6*, 622.

[16] M. Fereidoonnezhad, B. Kaboudin, T. Mirzaee, R. Babadi Aghakhanpour, M. Golbon Haghighi, Z. Faghih, Z. Faghih, Z. Ahmadipour, B. Notash, H. R. Shahsavari, *Organometallics* **2017**, *36*, 1707.

[17] J. Ruiz, C. Vicente, C. de Haro, A. Espinosa, *Inorg. Chem.* **2011**, *50*, 2151.

[18] G. Millán, N. Giménez, R. Lara, J. R. Berenguer, M. T. Moreno, E. Lalinde, E. Alfaro-Arnedo, I. P. López, S. Pineiro-Hermida, J. G. Pichel, *Inorg. Chem.* **2019**, *58*, 1657.

[19] M. Clemente, I. H. Polat, J. Albert, R. Bosque, M. Crespo, J. Granell, C. López, M. Martínez, J. Quirante, R. Messeguer, C. Calvis, J. Badía, L. Baldomà, M. Font-Bardia, M. Cascante, *Organometallics* **2018**, *37*, 3502.

[20] H. R. Shahsavari, N. Giménez, E. Lalinde, M. T. Moreno, M. Fereidoonnezhad, R. Babadi Aghakhanpour, M. Khatami, F. Kalantari, Z. Jamshidi, M. Mohammadpour, *Eur. J. Inorg. Chem.* **2019**, *2019*, 1360.

[21] M. Jamshidi, R. Yousefi, S. M. Nabavizadeh, M. Rashidi, M. G. Haghighi, A. Niazi, A.-A. Moosavi-Movahedi, *Int. J. Biol. Macromol.* **2014**, *66*, 86.

[22] M. Fereidoonnezhad, M. Niazi, Z. Ahmadipour, T. Mirzaee, Z. Faghih, Z. Faghih, H. R. Shahsavari, *Eur. J. Inorg. Chem.* **2017**, *2017*, 2247.

[23] H. Samouei, M. Rashidi, F. W. Heinemann, *J. Iran. Chem. Soc.* **2014**, *11*, 1207.

[24] E. Lalinde, R. Lara, I. P. López, M. T. Moreno, E. Alfaro-Arnedo, J. G. Pichel, S. Piñeiro-Hermida, *Chem. - a Eur. J.* **2018**, *24*, 2440.

[25] M. V. Babak, M. Pfaffeneder-Kmen, S. M. Meier-Menches, M. S. Legina, S. Theiner, C. Licona, C. Orvain, M. Hejl, M. Hanif, M. A. Jakupec, B. K. Keppler, C. Gaiddon, C. G. Hartinger, *Inorg. Chem.* **2018**, *57*, 2851.

[26] C. K. Koo, L. K. Y. So, K. L. Wong, Y. M. Ho, Y. W. Lam, M. H. W. Lam, K. W. Cheah, C. C. W. Cheng, W. M. Kwok, *Chem. - a Eur. J.* **2010**, *16*, 3942.

[27] A. Erxleben, *Curr. Med. Chem.* **2018**, *26*, 694.

[28] L. D. Zorova, V. A. Popkov, E. Y. Plotnikov, D. N. Silachev, I. B. Pevzner, S. S. Jankauskas, V. A. Babenko, S. D. Zorov, A. V. Balakireva, M. Juhaszova, S. J. Sollott, D. B. Zorov, *Anal. Biochem.* **2018**, *552*, 50.

[29] K. Han, Q. Lei, S. B. Wang, J. J. Hu, W. X. Qiu, J. Y. Zhu, W. N. Yin, X. Luo, X. Z. Zhang, *Adv. Funct. Mater.* **2015**, *25*, 2961.

[30] S. Fulda, L. Galluzzi, G. Kroemer, *Nat. Rev. Drug Discov.* **2010**, *9*, 447.

[31] D. Pathania, M. Millard, N. Neamati, *Adv. Drug Deliv. Rev.* **2009**, *61*, 1250.

[32] A. Muscella, N. Calabriso, F. P. Fanizzi, S. A. De Pascali, L. Urso, A. Ciccarese, D. Migoni, S. Marsigliante, *Br. J. Pharmacol.* **2008**, *153*, 34.

[33] K. Li, T. Zou, Y. Chen, X. Guan, C. M. Che, *Chem. - a Eur. J.* **2015**, *21*, 7441.

[34] T. Sun, X. Guan, M. Zheng, X. Jing, Z. Xie, *ACS Med. Chem. Lett.* **2015**, *6*, 430.

[35] K. Suntharalingam, Y. Song, S. J. Lippard, *Chem. Commun.* **2014**, *50*, 2465.

[36] S. P. Wisnovsky, J. J. Wilson, R. J. Radford, M. P. Pereira, M. R. Chan, R. R. Laposa, S. J. Lippard, S. O. Kelley, *Chem. Biol.* **2013**, *20*, 1323.

[37] J. Zajac, H. Kostrhunova, V. Novohradsky, O. Vrana, R. Raveendran, D. Gibson, J. Kasparkova, V. Brabec, *J. Inorg. Biochem.* **2016**, *156*, 89.

[38] Z. Guo, W. L. Tong, M. C. W. Chan, *Chem. Commun.* **2014**, *50*, 1711.

[39] J. Li, X. He, Y. Zou, D. Chen, L. Yang, J. Rao, H. Chen, M. C. W. Chan, L. Li, Z. Guo, L. W. Zhang, C. Chen, *Metallomics* **2017**, *9*, 726.

[40] R. V. Patel, B. Mistry, R. Syed, A. K. Rathi, Y. J. Lee, J. S. Sung, H. S. Shinf, Y. S. Keum, *Eur. J. Pharm. Sci.* **2016**, *88*, 166.

[41] K. Lemańska, H. Szymusiak, B. Tyrakowska, R. Zieliński, A. E. M. F. Soffers, I. M. C. M. Rietjens, *Free Radic. Biol. Med.* **2001**, *31*, 869.

[42] P. G. Pietta, *J. Nat. Prod.* **2000**, *63*, 1035.

[43] T. P. T. Cushnie, A. J. Lamb, *Int. J. Antimicrob. Agents* **2005**, *26*, 343.

[44] J. B. Harborne, C. A. Williams, *Phytochemistry* **2000**, *55*, 481.

[45] E. Middleton Jr., C. Kandaswami, T. C. Theoharides, *Pharmacol. Rev.* **2000**, *52*, 673.

[46] P. Batra, A. K. Sharma, *Biotechniques* **2013**, *3*, 1.

[47] M. M. Kasprzak, A. Erxleben, J. Ochocki, *RSC Adv.* **2015**, *5*, 45853.

[48] A. Kurzwernhart, S. Mokesch, E. Klapproth, M. S. Adib-Ravazi, M. A. Jakupec, C. G. Hartinger, W. Kandioller, B. K. Keppler, *Eur. J. Inorg. Chem.* **2016**, *2016*, 240.

[49] M. M. Dell'Anna, V. Censi, B. Carrozzini, R. Caliandro, N. Denora, M. Franco, D. Veclani, A. Melchior, M. Tolazzi, P. Mastrorilli, *J. Inorg. Biochem.* **2016**, *163*, 346.

[50] X. Qin, G. Xu, F. Chen, L. Fang, S. Gou, *Bioorg. Med. Chem.* **2017**, *25*, 2507.

[51] M. Fabijańska, K. Studzian, L. Szmigiero, A. J. Rybarczyk-Pirek, A. Pfitzner, B. Cebula-Obrzut, P. Smolewski, E. Zyner, J. Ochocki, *Dalton Trans.* **2015**, *44*, 938.

[52] M. Fabijańska, M. M. Kasprzak, J. Ochocki, *Int. J. Mol. Sci.* **2021**, *22*, 7568.

[53] T. A. Phan, X.-M. Yu, M. Kunnimalaiyaan, H. Chen, *J. Surg. Res.* **2011**, *170*, 84.

[54] K. Hu, W. Wang, H. Cheng, S. S. Pan, J. Ren, *Med. Chem. Res.* **2011**, *20*, 838.

[55] B. M. Mistry, R. V. Patel, Y. S. Keum, D. H. Kim, *Bioorg. Med. Chem. Lett.* **2015**, *25*, 5561.
[56] J. Marques, A. M. S. Silva, M. P. M. Marques, S. S. Braga, *Inorg. Chim. Acta* **2019**, *488*, 71.
[57] J. D. S. S. Yadav, J. D. Singh, *J. Biomol. Struct. Dyn.* **2019**, *37*, 3337.
[58] A. R. Rubio, R. González, N. Busto, M. Vaquero, A. L. Iglesias, F. A. Jalón, G. Espino, A. M. Rodríguez, B. García, B. R. Manzano, *Pharmaceutics* **2021**, *13*, 1540.
[59] M. E. Casida, C. Jamorski, K. C. Casida, D. R. Salahub, *J. Chem. Phys.* **1998**, *108*, 4439.
[60] K. Suresh Babu, T. Hari Babu, P. V. Srinivas, K. Hara Kishore, U. S. N. Murthy, J. M. Rao, *Bioorg. Med. Chem. Lett.* **2006**, *16*, 221.
[61] M. S. Lowry, W. R. Hudson, R. A. Pascal, S. Bernhard, *J. am. Chem. Soc.* **2004**, *126*, 14129.
[62] *SAINT* v8.37, Bruker-AXS (2016), APEX3 V2016.1.0. Madison, Wisconsin, USA.
[63] L. Krause, R. Herbst-Irmer, G. M. Sheldrick, D. Stalke, *J. Appl. Cryst.* **2015**, *48*, 3.
[64] L. J. Farrugia, *J. Appl. Cryst.* **2012**, *45*, 849.
[65] G. M. Sheldrick, SHELX-2016, Program for Crystal Structure Refinement, University of Göttingen, Göttingen, **2016**.
[66] A. D. Becke, *J. Chem. Phys.* **1993**, *98*, 5648.
[67] C. Lee, W. Yang, R. G. Parr, *Phys. Rev. B* **1988**, *37*, 785.
[68] Gaussian 09 (Revision C.01), M. J. Frisch, G. W. Trucks, H. B. Schlegel, G. E. Scuseria, M. A. Robb, J. R. Cheeseman, G. Scalmani, V. Barone, B. Mennucci, G. A. Petersson, H. Nakatsuji, M. Caricato, X. Li, H. P. Hratchian, A. F. Izmaylov, J. Bloino, G. Zheng, J. L. Sonnenberg, M. Hada, M. Ehara, K. Toyota, R. Fukuda, J. Hasegawa, M. Ishida, T. Nakajima, Y. Honda, O. Kitao, H. Nakai, T. Vreven, J. A. Montgomery, Jr., J. E. Peralta, F. Ogliaro, M. Bearpark, J. J. Heyd, E. Brothers, K. N. Kudin, V. N. Staroverov, R. Kobayashi, J. Normand, K. Raghavachari, A. Rendell, J. C. Burant, S. S. Iyengar, J. Tomasi, M. Cossi, N. Rega, J. M. Millam, M. Klene, J. E. Knox, J. B. Cross, V. Bakken, C. Adamo, J. Jaramillo, R. Gomperts, R. E. Stratmann, O. Yazyev, A. J. Austin, R. Cammi, C. Pomelli, J. W. Ochterski, R. L. Martin, K. Morokuma, V. G. Zakrzewski, G. A. Voth, P. Salvador, J. J. Dannenberg, S. Dapprich, A. D. Daniels, Ö. Farkas, J. B. Foresman, J. V. Ortiz, J. Cioslowski, and D. J. Fox, *Gaussian, Inc.*, Wallingford CT, **2009**.
[69] P. J. Hay, W. R. Wadt, *J. Chem. Phys.* **1985**, *82*, 299.
[70] W. J. Hehre, K. Ditchfield, J. A. Pople, *J. Chem. Phys.* **1972**, *56*, 2257.
[71] M. M. Francl, W. J. Pietro, W. J. Hehre, J. S. Binkley, M. S. Gordon, D. J. DeFrees, J. A. Pople, *J. Chem. Phys.* **1982**, *77*, 3654.
[72] S. Grimme, S. Ehrlich, L. Goerigk, *J. Comput. Chem.* **2011**, *32*, 1456.
[73] S. Grimme, J. Antony, S. Ehrlich, H. Krieg, *J. Chem. Phys.* **2010**, *132*, 154104.
[74] A. V. Marenich, C. J. Cramer, D. G. Truhlar, *J. Phys. Chem. B* **2009**, *113*, 6378.
[75] C. Jamorski, M. E. Casida, D. R. Salahub, *J. Chem. Phys.* **1996**, *104*, 5134.
[76] M. Petersilka, U. J. Gossmann, E. K. U. Gross, *Phys. Rev. Lett.* **1996**, *76*, 1212.
[77] E. Zafon, I. Echevarría, S. Barrabés, B. R. Manzano, F. A. Jalón, A. M. Rodríguez, A. Massaguer, G. Espino, *Dalton Trans.* **2021**, *51*, 111.
[78] S. W. Lai, M. C. W. Chan, K. K. Cheung, S. M. Peng, C. M. Che, *Organometallics* **1999**, *18*, 3991.
[79] J. Y. Cho, K. Y. Suponitsky, J. Li, T. V. Timofeeva, S. Barlow, S. R. Marder, *J. Organomet. Chem.* **2005**, *690*, 4090.
[80] A. F. Rausch, U. V. Monkowius, M. Zabel, H. Yersin, *Inorg. Chem.* **2010**, *49*, 7818.
[81] A. Diez, J. Forniés, A. García, E. Lalinde, M. T. Moreno, *Inorg. Chem.* **2005**, *44*, 2443.
[82] O. J. Stacey, J. A. Platts, S. J. Coles, P. N. Horton, S. J. A. Pope, *Inorg. Chem.* **2015**, *54*, 6528.
[83] L. Fuks, K. Samochocka, R. Anulewicz-Ostrowska, M. Kruszewski, W. Priebe, W. Lewandowski, *Eur. J. Med. Chem.* **2003**, *38*, 775.
[84] M. Akkoç, S. Demirel, E. Öz, S. Altın, A. Bayri, V. Dorcet, T. Roisnel, C. Bruneau, İ. Özdemir, S. Yaşar, *Polyhedron* **2019**, *157*, 434.
[85] A. Aliprandi, D. Genovese, M. Mauro, L. De Cola, *Chem. Lett.* **2015**, *44*, 1152.
[86] J. S. Field, R. J. Haines, D. R. McMillin, G. C. Summerton, *J. Chem. Soc. Dalton Trans.* **2002**, 1369.
[87] V. V. Sivchik, E. V. Grachova, A. S. Melnikov, S. N. Smirnov, A. Y. Ivanov, P. Hirva, S. P. Tunik, I. O. Koshevoy, *Inorg. Chem.* **2016**, *55*, 3351.
[88] J. Brooks, Y. Babayan, S. Lamansky, P. I. Djurovich, I. Tsyba, R. Bau, M. E. Thompson, *Inorg. Chem.* **2002**, *41*, 3055.
[89] M. Ghedini, T. Pugliese, M. La Deda, N. Godbert, I. Aiello, M. Amati, S. Belviso, F. Lelj, G. Accorsi, F. Barigelletti, *Dalton Trans.* **2008**, 4303.
[90] D. Wang, X. Chen, H. Yang, D. Zhong, B. Liu, X. Yang, L. Yue, G. Zhou, M. Ma, Z. Wu, *Dalton Trans.* **2020**, *49*, 15633.
[91] F. Niedermair, O. Kwon, K. Zojer, S. Kappaun, G. Trimmel, K. Mereiter, C. Slugovc, *Dalton Trans.* **2008**, 4006.
[92] S. Sprouse, K. A. King, P. J. Spellane, R. J. Watts, *J. am. Chem. Soc.* **1984**, *106*, 6647.
[93] B. Longato, G. Bandoli, A. Dolmella, *Eur. J. Inorg. Chem.* **2004**, *2*, 1092.
[94] J. A. Broomhead, D. P. Fairlie, M. W. Whitehouse, *Chem-BiolInteract* **1980**, *31*, 113.
[95] L. K. McKenzie, H. E. Bryant, J. A. Weinstein, *Coord. Chem. Rev.* **2019**, *379*, 2.
[96] M. Obata, S. Hirohara, R. Tanaka, I. Kinoshita, K. Ohkubo, S. Fukuzumi, M. Tanihara, S. Yano, *J. Med. Chem.* **2009**, *52*, 2747.
[97] A. Naik, R. Rubbiani, G. Gasser, B. Spingler, *Angew. Chemie* **2014**, *126*, 7058.
[98] F. Qi, H. Yuan, Y. Chen, Y. Guo, S. Zhang, Z. Liu, W. He, Z. Guo, *J. Inorg. Biochem.* **2021**, *218*, 5.

[99] R. E. Doherty, I. V. Sazanovich, L. K. McKenzie, A. S. Stasheuski, R. Coyle, E. Baggaley, S. Bottomley, J. A. Weinstein, H. E. Bryant, *Sci. Rep.* **2016**, *6*, 22668.
[100] Z. H. Siddik, *Oncogene* **2003**, *22*, 7265.
[101] H. S. Kim, Y. S. Lee, D. K. Kim, *Pharmacology* **2009**, *84*, 300.
[102] P. E. Porporato, N. Filigheddu, J. M. B. S. Pedro, G. Kroemer, L. Galluzzi, *Cell Res.* **2018**, *28*, 265.
[103] L. Dalla Via, A. N. García-Argáez, A. Adami, S. Grancara, P. Martinis, A. Toninello, D. Belli Dell'Amico, L. Labella, S. Samaritani, *Bioorg. Med. Chem.* **2013**, *21*, 6965.
[104] M. Hyeraci, V. Scalcon, A. Folda, L. Labella, F. Marchetti, S. Samaritani, M. P. Rigobello, L. Dalla Via, *ChemMedChem* **2021**, *16*, 1956.

SUPPORTING INFORMATION

Additional supporting information can be found online in the Supporting Information section at the end of this article.

How to cite this article: J. Leal, G. Durá, F. A. Jalón, E. Zafon, A. Massaguer, J. V. Cuevas, L. Santos, A. M. Rodríguez, B. R. Manzano, *Appl Organomet Chem* **2023**, *37*(3), e6983. https://doi.org/10.1002/aoc.6983